UV LINE DIAGNOSTICS OF ACCRETION DISK WINDS IN CATACLYSMIC VARIABLES

Peter Vitello

Physics Department

Lawrence Livermore National Laboratory

Livermore, CA 94550

and

Isaac Shlosman

Department of Physics and Astronomy

University of Kentucky

Lexington, KY 40506-0055

ABSTRACT

The *IUE* database is used to analyze the UV line shapes of cataclysmic variables RW Sex, RW Tri and V Sge. Observed lines are compared to synthetic line profiles computed using a model of rotating bi-conical winds from accretion disks. The wind model calculates the wind ionization structure self-consistently including photoionization from the disk and boundary layer and treats 3-D line radiation transfer in the Sobolev approximation. It is found that winds from accretion disks provide a good fit for reasonable parameters to the observed UV lines which include the P Cygni profiles for low-inclination systems and pure emission at large inclination. Disk winds are preferable to spherical winds which originate on the white dwarf because they (1) require a much lower ratio of mass loss rate to accretion rate and are therefore more plausible energetically, (2) provide a natural source for a bi-conical distribution of mass outflow which produces strong scattering far above the disk leading to P Cygni profiles for low-inclination systems, and pure line emission profiles at high inclination with the absence of eclipses in UV lines, and (3) produce rotation-broadened pure emission lines at high inclination.

1. Introduction

A cataclysmic variable system (hereafter CV) consists, by definition, of a white dwarf (WD) primary, and a secondary late-type main sequence star. An important characteristic of a CV is the mass transfer within the system, which (if the primary is non-magnetic) results in the formation of an accretion disk around the primary in the orbital plane of the binary. Such a disk may become the prime source of UV and optical light generated by the system. Additional photons come from the WD, from the secondary, and from the interfaces of the disk with the WD (*i.e.* the boundary layer), and with the accretion stream from the secondary (the 'hot' spot). At different evolutionary stages, CVs are observed to experience outflows. The latter may have a substantial optical depth in the resonance lines of abundant elements and hence will contribute to the observed line spectrum.

Non-magnetic CVs can be divided into two main groups: nova-like variables and dwarf novae (*e.g.* Verbunt 1987). The former spend most of their time in the bright state, while the latter experience outbursts of 2–5 magnitudes. Continuum spectra of these objects show a clear signature of optically thick accretion disks which correspond to large accretion rates, $\dot{M}_a \gtrsim 10^{-9}$ $M_\odot$ yr^{-1}. Theoretically such an accretion disk and its boundary layer (BL) are expected to dominate the energy output from a CV in the UV/EUV band, *i.e.* at 200–2,000Å. Observations by the *International Ultraviolet Explorer* (*IUE*) satellite and *Voyager* spacecraft, which are currently the prevailing sources of information in this energy band, have confirmed this in some cases (*e.g.* Polidan, Mauche and Wade 1990). These observations have also shown clear evidence for high-velocity winds from nova-like variables and erupting dwarf novae, and suggest their accretion disk origin (see Córdova 1986 and Drew 1991 for recent reviews). Signature of an outflow has been seen also at optical frequencies (*e.g.* Honeycutt, Schlegel and Kaitchuck 1986; Marsh and Horne 1990).

Clues to the wind geometry come from the sensitivity of the UV high-ionization line spectra (CIV λ1549, SiIV λ1397 and NV λ1240) to the inclination angle of the system. The P Cygni profiles with a blueshifted absorption and a redshifted emission are prominent in

the low-to-intermediate ($\lesssim 65°$) inclination systems, especially those with high accretion rates, *e.g.* in RW Sex (Greenstein and Oke 1982), V3885 Sgr (Guinan and Sion 1982), TW Vir (Córdova and Mason 1982), RX And (Klare *et al.* 1982) and others (Mauche, Córdova and Verbunt 1988). During the low-luminosity state of dwarf novae or in high inclination (eclipsing) systems the UV lines appear broad and highly symmetric (gaussian), while the absorption component vanish (Frank *et al.* 1981). The fact that the CIV line is affected much less than the UV continuum during the eclipses of the primary and the inner disk by the companion (*e.g.* in RW Tri, DQ Her), indicates that the UV line-emitting material extends well above the disk (*e.g.* King *et al.* 1983; Córdova and Mason 1985; Naylor *et al.* 1988). The UV resonant intensities also imply that these lines have a substantial optical depth (Drew and Verbunt 1985). The UV line ratios (King *et al.* 1983) and the difference in variation of fluxes in the CIV and NV lines during the eclipse supports an X-ray photoionization nebula type model for the wind as opposite to the ionization structure being due to collisional ionization in a hot wind (Kallman 1983; Córdova and Mason 1985).

Early estimates of the mass loss rates, $\dot{M}_w$, from nova-like variables and dwarf-novae in outburst have been made on the basis of comparison of observed line shapes with theoretical lines calculated for early-type stars (*e.g.* Krauter *et al.* 1981; Córdova and Mason 1982, Klare *et al.* 1982). It has been argued that the presence of a luminous accretion disk, which can act both as a source of the wind and of radiation pressure on the wind, will introduce a bi-conical geometry into the outflow. In addition to its dynamical effects, the occultation, scattering, and ionization by the disk radiation field will lead to a bi-polar emission line emissivity distribution even if the wind outflow was spherical (Drew 1987). Typical published line spectra of CVs which show blueshifted absorption, have deepest absorption close to the line center, roughly within $\sim 1,000$ km s^{-1} from the rest frame of the system. This is contrary to the absorption line shapes of the spherical winds from OB stars which generally have smallest residual flux at the blue edge. Such a difference in the line shape imposes a constraint on the wind: a large column density of absorbers

must exist along the line of sight to the observer and close to the base of the wind, but the wind should become optically thin before reaching terminal velocity. As mentioned in the works on CV line fitting (Drew 1987; Mauche and Raymond 1987), this points towards a slowly accelerating velocity law for an outflow.

CV wind mass loss rates have recently been calculated from synthesized model UV resonance line profiles which include the non-spherical nature of the disk radiation field (Drew 1987; Mauche and Raymond 1987; Drew, Hoare and Woods 1991). These studies share the assumptions that the wind itself is radially driven from the WD. However, mass loss rates for spherical winds which are required to explain observations appear to be a large fraction of the accretion rate *e.g.* $\dot{M}_w / \dot{M}_a \gtrsim 1/3$ (Mauche and Raymond 1987). Such extensive winds can be hardly justified if driven by radiation pressure. We find, however, that if one relaxes the assumption that the wind originates from the WD and instead accounts for the mass loss from the extended disk surface, the energy constraint appears to be far less stringent. We demonstrate below that disk winds allow for greatly reduced mass loss rates. Therefore, all estimates for $\dot{M}_w$ from CVs published previously must be used with reservation only.

This paper makes use of the *IUE* database to analyze the line shapes of three CVs, RW Sex, RW Tri and V Sge, and compares the observed lines with the synthetic line profiles from bi-conical rotating accretion disk winds calculated using a three-dimensional radiation transfer in the Sobolev approximation (Sobolev 1957; Rybicki and Hummer 1978; 1983). Only the most necessary details of the numerical method are presented below. A full account of the numerical model is given in Shlosman and Vitello (1992). We find that the introduction of a non-radial rotating wind provides a more realistic representation, and results in good fits to the observed line profiles simultaneously in absorption and emission. Furthermore, rotation has a profound effect on the emission part of the line which broadens the line width and can lead to asymmetries. Such structure may possibly be confirmed by future high-resolution observations with the Hubble Space Telescope.

The archive data used in this study is described in section 2. In section 3 we survey the observational status of modeled CV systems. Section 4 explains briefly the kinematic and radiation-transfer model of the wind as well as the calculation of synthetic lines. The comparison of synthetic and observed lines is done in section 5 and conclusions are drawn in section 6.

2. Data Analysis

The *IUE* archive low-resolution spectra used in this study have been obtained with the Short Wavelength Prime (SWP) camera covering between 1,150–1,950 Å. Only large aperture spectra have been used to avoid possible errors in centering. The effective SWP resolution at 1,550Å is $\sim$ 4.5–5 Å (Cassatella, Barbero and Benvenuti 1985). To allow for this instrumental broadening our profiles were smoothed with a gaussian of FWHM $\sim$ 4.5 Å. The technical and performance characteristics of the *IUE* telescope and the instrumentation are given by Boggess *et al.* (1978).

We have used the *IUE* data archive spectra for dwarf novae and nova-like stars selected from the CV Catalogue (Ritter 1990). A comprehensive overview of low-resolution spectra for these objects can be found also in LaDous (1990). Below we present the results for three nova-like CVs. Synthetic spectra for dwarf novae in outburst will be published elsewhere. The data was retrieved and reduced *in situ* by using the standard reduction package at the *IUE* Regional Data Analysis Facility at the University of Colorado. The data set consists of 16 low resolution spectra of RW Tri, RW Sex and V Sge. The details of observations are summarized in Table I. The SWP image numbers are listed in column (2), the dates and exposure times appear in columns (3) and (4), and the orbital phase is given in (5). All SWPs used in this work appear to be taken during the normal state of the nova-like variables, as confirmed by Ritter (1990). Note that uncertainties in the distances to CVs dominate the calibration errors of the observed fluxes. We have attempted to fit only the line profiles. The interstellar reddening, therefore, is ignored because it would not affect

the line-to-continuum flux ratio.

3. Observations of Nova-Like Variables

The optical and UV fluxes from nova-like variables usually show only weak (around one magnitude) variability. This would imply that these systems spend most of their time in dynamical equilibrium. The latter and the availability of *IUE* archive line spectra made them attractive for our modeling.

(a) *RW Sextantis* ($BD - 7°3007$)

This is a bright (non-eclipsing) nova-like variable with an orbital period of 5.93 hours. P Cygni line profiles are present in the UV spectrum indicating an outflow with absorption in NV and CIV (with residual flux at 11% of the continuum) blueshifted by 3,000 km s^{-1} and the absorption wing extending to $-4,500$ km s^{-1} (Greenstein and Oke 1982). The distance is calculated to be 120–400 pc (Warner 1967; Greenstein and Oke 1982; Patterson 1984; Bolick *et al.* 1987). The CV's visual magnitude varies between 10.4–10.8 (Polidan, Mauche and Wade 1990). The mass of the primary is in the range 0.81 ± 0.045 $M_\odot$, and that of the secondary 0.54 ± 0.09 $M_\odot$ (Bolick *et al.* 1987). This gives a mass ratio of roughtly $q \simeq 0.7$. The inclination angle to the observer, $i = 32°$–$54°$, has been estimated by Bolick *et al.* from continuum fitting using a standard accretion disk model. Because this system is so bright and shows little variation, it is resonable to assume that the disk and the boundary layer are optically thick and have reached thermal equilibrium (Polidan, Mauche and Wade 1990). The accretion rate is calculated by Bolick *et al.* to be $\sim$ 3–5×10^{-9} $M_\odot$ yr^{-1}, with the outer disk radius $\sim$ 2–4×10^{10} cm. Greenstein and Oke (1982) determine a higher accretion rate, 1–3×10^{-8} $M_\odot$ yr^{-1}. The effective temperature of the WD is limited to below 50,000 °K (Patterson 1984; Bolick *et al.* 1987).

(b) *RW Trianguli*

This CV is a bright (m_V =12–14 Patterson 1984) eclipsing member of UX UMa class of nova-like variables with a 5.57 hour binary period. The CIV emission line shows a blue

asymmetry (the blue wing is more extended than the red one) with its peak redshifted (3–4 Å, as well as the peaks of NV and SiIV), while the centroid of the emission is approximately at the rest wavelength (Córdova and Mason 1985). The UV lines do not change substantially during the eclipse: CIV and NV decrease by 15–20% and SiIV decreases by 60%. This indicates that the line emission must come from an extended volume. The CIV, NV and SiIV lines are observed only in emission and their shapes do not change appreciable with the orbital phase, even during the eclipse (Córdova and Mason 1985).

Frank and King (1981) estimate the inclination angle, $i = 82^{o}$, the mass $M_{WD} \sim 1.3 M_{\odot}$, and other basic parameters of the system from fitting the continuum spectrum using a standard accretion disk model. The total UV to near-IR luminosity is $1.5 L_{\odot}$, using the distance 250 pc derived by Bailey (1981). However, this distance (as well as the mass determination for the secondary — see Ritter 1990) depends upon the assumption that the secondary is a main sequence M0 star, which is in contradiction with the CCD spectra obtained by Young and Schneider (1981). Horne and Stieging (1985) give as their best fit distance of $\sim$ 500 pc.

Kaitchuck *et al.* (1983) have estimated the inclination angle for this system as 67^{o}–75^{o} using radial velocity curve (K velocity) data and give the WD and secondary mass respectively as being in the range 0.46–0.74 $M_{\odot}$ and 0.68–0.77 $M_{\odot}$. Horne and Stiening (1985) question the accuracy of both papers: the Frank and King (1981) results are critisized due to their neglect of interstellar extinction (the *IUE* ultra-violet data was not available at the time of 1981 paper), and that of Kaitchuck *et al.* (1983), because their K velocity may be too large due to non-circular streamlines in the outer disk region. A smaller K velocity would imply a larger inclination and a more massive primary. The eclipse mapping of RW Tri by Horne and Stiening (1985) is not sensitive to the mass ratio and, consequently, rather a wide range was suggested for the white dwarf mass: 0.6–1.4 $M_{\odot}$ with the corresponding inclination angle range 72^{o}–79^{o}.

Calculated values for the accretion rate depend upon the use of model atmosphere

(*e.g.* Wade 1984, 1990a) or disk blackbody continuum model spectra. In addition, the slope of the UV continuum is very insensitive to the $\dot{M}_a$ and its estimates in the literature based on this property are subject to large errors (*e.g.* Verbunt 1987).

Using spectral fits to the continuum Frank and King (1981) have calculated the accretion rate $9\times10^{-10}-4\times10^{-9}\mathrm{M}_\odot\,\mathrm{yr}^{-1}$ for a blackbody disk. Córdova and Mason (1985) estimate the accretion rate to be $1.4\times10^{-9}(\mathrm{M}_{WD}/0.7\mathrm{M}_\odot)^{-1}(R_{WD}/5\times10^8\mathrm{cm})^3\mathrm{M}_\odot\,\mathrm{yr}^{-1}$ for a blackbody disk and $1.6\times10^{-10}\mathrm{M}_\odot\,\mathrm{yr}^{-1}$ for a model atmosphere disk. Eclipse mapping is independent of spectral fits to the continuum (Horne 1983) and has been used by Horne and Stiening (1985) to determine the RW Tri accretion rate as being 5×10^{-9}–3×10^{-8} $\mathrm{M}_\odot$ yr^{-1}. This is in general agreement with other members of UX UMa subclass CVs which accrete at $\dot{M}_a \gtrsim 10^{-9}$ $\mathrm{M}_\odot$ yr^{-1}.

(c) *V Sagittae*

Few studies have been made of the anomalously bright eclipsing system V Sge which has period of 12.34 hours. The visual magnitude of this system varies between $m_V \sim 9-13$ and from interstellar extinction its distance estimated to be roughly 1.2 kpc (Herbig *et al.* 1965; Koch *et al.* 1986; Ritter 1990). The light curve of this system is complex, making the application of formal models difficult. The radial velocity data of Herbig *et al.* (1965), derived using the OIII λ 3132 and λ3444 emission lines, suggests a secondary-to-primary mass ratio $q \simeq 3.77$. For the secondary on or near the main sequence and filling its Roche lobe this implies that the mass of the primary is 0.74 $M_\odot$, and that of the secondary is 2.8 $\mathrm{M}_\odot$. For this large of a mass ratio, mass transfer is likely to be occuring on a thermal time-scale with the accretion rate $\dot{M}_a \simeq 5\times10^{-7}\mathrm{M}_\odot\,\mathrm{yr}^{-1}$ (Williams *et al.* 1986).

The UV lines in V Sge, in general, do not show eclipse effects, supporting the general picture of the line emitting material being situated well above the disk. Partial UV line eclipses have been observed (Koch *et al.* 1986; Williams *etal.* 1986). The absence of any forbidden lines implies that the electron density $\log n_e > 10.5$ cm^{-2} in the emission region. Sharing a similar trend for all high inclination systems, there is no evidence of absorption

in the observed in the UV emission lines, which all are predominately symmetric and redshifted by the same amount (Koch *et al.* 1986). Optical observations indicated that this is an eclipsing binary and its inclination angle is clearly large, but poorly known. For our modeling we have adopted the value of 90^o given by Ritter (1990), which is consistent with the data of Herbig *et al.* (1965).

4. Synthetic Line Modeling

Both nova-like stars and erupting dwarf novae experience winds with velocities up to 5,000 km s^{-1}, which are evident from the blueshifted absorption in the UV spectra of these objects. The driving mechanism behind the wind from a CV is still undecided. Two possibilities have been suggested so far: line-driven winds (Krautter *et al.* 1981; Córdova and Mason 1982, 1985; Drew and Verbunt 1985), and magnetically-driven winds (Pudritz and Norman 1986; Cannizzo and Pudritz 1988; see also Emmering, Blandford and Shlosman 1992 for MHD winds from disks in active galactic nuclei). Theoretical modeling provides some support to the view that radiation pressure in lines is the driving force behind the wind (Drew and Verbunt 1985; Kallman and Jensen 1985; Drew 1987; Mauche and Raymond 1987; Vitello and Shlosman 1988, hereafter Paper I; Shlosman and Vitello 1992, hereafter Paper II). The theory of the line-driven winds (LDWs) from accretion disks in CVs and AGNs has been developed in Paper I, in close analogy with the winds from OB stars, but no attempt to fit line profiles was made. As we have stated in section 1, only radial non-rotating winds centered on the WD have been considered so far for this purpose, although the radiation field has been treated to the full extent (Drew 1987; Mauche and Raymond 1987). In the accompanying paper, we attempt to close the gap between the theory and observations by performing a parameter study of line profiles for the ionization structure of the wind for non-radial LDWs from keplerian accretion disks, based on the kinematic and line-transfer model developed by us. Here we only discuss the basic assumptions that are relevant for fitting the synthetic line profiles to the observed

UV lines from a number of nova-like variables.

(a) *Modeling Wind Kinematics*

The typical accretion rate onto a WD can be estimated indirectly from the bolometric luminosity of the CV,

$$\dot{M}_a \sim 4 \times 10^{-9} \left(\frac{L_{bol}}{10 L_\odot}\right) \left(\frac{R_{WD}}{7 \times 10^8 \mathrm{cm}}\right) \left(\frac{M_{WD}}{0.7 M_\odot}\right)^{-1} M_\odot \, \mathrm{yr}^{-1}, \quad (1)$$

where M_{WD} and R_{WD} are the WD mass and radius respectfully. Hamada and Salpeter (1961) provide a relationship between the mass and radius for different chemical compositions of the WD. The accretion rates for nova-like variables indicate a rather a high rate of mass transfer compared to other type CVs. The mass loss by the wind is estimated from observations and from an assumption of a 'single scattering' limit to be $\dot{M}_w \gtrsim 10^{-10}$ $M_\odot$ yr^{-1} (*e.g.* Guinan and Sion 1982; Córdova and Mason 1982; Drew 1987; Mauche and Raymond 1987).

As a first step towards our comparison of the observed and calculated line profiles we have made several simplifying assumptions about the wind kinematics. First, a cylindrical system of coordinates is used because of the prevailing axial symmetry in the problem. The z-axis is aligned with the rotation axis of the disk, and r and ϕ are the radial and azimuthal coordinates on the surface of the disk which is assumed to be planar. The wind streamlines are taken to be 3-D spirals which start at the disk surface and continue at a constant angle, θ, to the rotation axis, *i.e.* the streamlines lie on conical surfaces. The conical angle for a particular streamline is taken to vary linearly with the initial radius of the streamline on the disk, $\theta = \theta_{min} + (\theta_{max} - \theta_{min})\tilde{r}$. Here $\tilde{r} \equiv (r_o - r_{min})/(r_{max} - r_{min})$, where r_o is the coordinate of the base of the streamline in the plane of the disk. The limiting inclination angles of bi-conical wind, θ_{min} and θ_{max}, occur at the inner and outer boundaries of the wind, r_{min} and r_{max}, which are calculated using temperature criterion (see below). This geometry is shown schematically in Figure 1. The velocity in the wind is given in terms of its cylindrical components, v_r, v_ϕ, v_z. Along each streamline $v_r = v_l \sin\theta$

and $v_z = v_l \cos\theta$, where v_l (which is the velocity in the rz plane), is assumed to be given by a power law function of $l = (z^2 + (r - ro)^2)^{1/2}$ (the distance from the disk along the cone),

$$v_l = v_o + (v_\infty - v_o)\left[\frac{(l/R_v)^\alpha}{(l/R_v)^\alpha + 1}\right]. \qquad (2)$$

The wind parameters v_o and v_∞ are the initial and asymptotic wind velocities along the streamline. R_v is the wind acceleration scale height, and α is the power law constant. The asymptotic velocity was assumed to scale with the *local* escape velocity, $v_{esc} = (2GM_{WD}/r_o)^{1/2}$, at the base of the streamline. For v_o we use 6 km s^{-1}. The wind orbital velocity is given initially by Keplerian motion, $v_{\phi,o} = (GM_{WD}/r_o)^{1/2}$. The wind is then assumed to conserve its specific angular momentum around the rotation axis, *i.e.* $v_\phi r = v_{\phi,o} r_o$. The mass loss per unit surface of the disk in the direction of a streamline is taken to be constant. Modifications of this mass loss distribution have been studied, and are considered in Paper II.

(b) *Wind Radiation Transport Modeling*

Contrary to the P Cygni line formation in the winds from OB stars, the continuum photons and the winds in CVs originate from an extended surface of accretion disk, not necessarily from the vicinity of the WD. In this non-spherical geometry, rotation, as well as aspect angle to the observer, i, have a profound effect on both the wind and the observed line spectrum. Differences between LDWs from disks and early-type stars are explored in Papers I and II.

Our line radiation transport model in the wind is based on the Sobolev method for a 3-D geometry developed by Rybicki and Hummer (1978; 1983). We consider radiation that propagates in a cylindrically symmmetric system with the 3-D velocity field described above. We calculate the line spectrum by evaluating the scattered luminosity from the wind and the net unscattered luminosity from the disk separately. To do so the surface of the disk, the BL and the WD are divided into radial and angular zones (with typically

100×100 points) each having a given intensity which contributes to the continuum radiation field. To account for the resonance line scattering above the disk, the z-axis was divided into zones as well (again typically 100 points). The rz-grid was zoned logarithmically and extends up to a distance of $500 R_{WD}$.

The disk is assumed to be optically thick as long as its local blackbody temperature (*e.g.* Shakura and Sunyaev 1973)

$$T_{disk}(x_o) = 1.1 \times 10^5 \left(\frac{M_{WD}}{0.7 \mathrm{M}_\odot}\right)^{1/4} \left(\frac{\dot{M}_a}{10^{-8} \mathrm{M}_\odot \ \mathrm{yr}^{-1}}\right)^{1/4} \left(\frac{R_{WD}}{7 \times 10^8 \mathrm{cm}}\right)^{-3/4}$$
$$x_o^{-3/4}(1 - x_o^{-1/2})^{1/4} \ ^\circ\mathrm{K} \qquad (3)$$

exceeds 8,000 °K, which defines also the outer disk radius. Here $x_o \equiv r_o / R_{WD}$. Because we limit ourselves to discussion of non-magnetic CVs, the disk can be assumed to extend to the surface of the WD. An additional assumption used in our models is that the wind originates in the part of the disk where the temperature varies between $10,000 - 50,000$ °K (Abbott 1982; Paper I). Limb darkening is included by weighting the blackbody intensity by the factor $2/5(1 + 3/2 \cos\theta)$, where θ is the angle with the z-axis as defined above (see Mauche and Raymond 1987).

The BL was assumed optically thick and emitting a blackbody spectrum as well. Patterson and Raymond (1985) gave a prescription for the BL temperature and height assuming a 45° tilt of its emitting surface with respect to the disk. The effective temperature of the BL under is

$$T_{BL} = 2 \times 10^5 \left(\frac{\dot{M}_a}{10^{-8} \mathrm{M}_\odot \ \mathrm{yr}^{-1}}\right)^{0.18} \left(\frac{M_{WD}}{0.7 \mathrm{M}_\odot}\right)^{0.86} \ ^\circ\mathrm{K}, \qquad (4)$$

and its radial and vertical (above the equatorial disk plane) extentions are

$$\left(\frac{H_{BL}}{R_{WD}}\right)^2 \approx 6.29 \times 10^{-4} \left(\frac{M_{WD}}{0.7 \mathrm{M}_\odot}\right)^{-0.85} \left(\frac{\dot{M}_a}{10^{-8} \mathrm{M}_\odot \ \mathrm{yr}^{-1}}\right)^{0.22} +$$
$$4.61 \times 10^{-4} \left(\frac{M_{WD}}{0.7 \mathrm{M}_\odot}\right)^{0.8} \left(\frac{\dot{M}_a}{10^{-8} \mathrm{M}_\odot \ \mathrm{yr}^{-1}}\right). \qquad (5)$$

The contribution of the WD to the radiation field above the disk is negligible for the range of WD temperatures considered here. We use equation (5) to estimate the height of the boundary layer, but leave its effective temperature as a free parameter.

The ionization at a particular point in the wind is calculated by assuming a constant temperature in the wind $\sim 20,000$ °K (*e.g.* King *et al.* 1983) and local ionization equilibrium. All ions of H, He, C, N, and O are considered with abundances by number relative to H given by their solar values: $N_{He}/N_H = 0.10, N_C/N_H = 3.72 \times 10^{-4}, N_N/N_H = 1.15 \times 10^{-4}$ and $N_O/N_H = 6.76 \times 10^{-4}$ (Withbroe 1971). Photoionization by UV photons from the disk, the BL and the WD was calculated self-consistently, taking into account the full 3-D radiation field. Collisional ionization and (three-body and dielectronic) recombination (with density-dependent effects) processes are included in the modeling, as well as radiative recombination.

The scattered contribution to the line luminosity is calculated using the volume integral formalism of Rybicki and Hummer (1983). Absorption is modeled by tracing rays from the discretized zones on the disk in the direction $\hat{n}$ to the observer and reducing the initial intensity by $e^{-\tau_S}$, where τ_S is the Sobolev optical depth, whenever the ray crosses a resonant velocity surface. Resonant surfaces at observer frequency ν occur whenever the condition $\nu - \nu_o - \nu_o \hat{n} \cdot (\vec{v}/c) = 0$ is satisfied, with ν_o being the line rest frame frequency and c the speed of light. Due to rotation, multiple resonant velocity surfaces may exist along the observers line on sight through the wind. Because the disk is taken as being optically thick, part of the wind is obscured at small and intermediate aspect angles, thus enhancing the line asymmetry. The source function is obtained by assuming a single resonant velocity surface. From a study of a topology of the resonant velocity surfaces, we estimate that secondary scattering contributions and blockage would not appreciable modify the source function. The source function is approximated as being due to scattered photons only, which results from the ratio of collisional to radiative radiative de-excitation being very small (see Kallman 1983). We also ignore the doublet structure of CIV line.

For comparison purposes, a 1-D spherical wind model was developed. This model is based on our 3-D disk model, but has a spherical density profile, streamlines which are radial from the center of the white dwarf, and $v_\phi = 0$. The distance l in the velocity law is now taken to be the radial distance surface from the white dwarf. Further details can be found in Paper II.

5. Synthetic Line Fitting to Observations

The goal of this paper is to show that UV lines in spectra of CVs can be matched by the synthetic line profiles calculated on the basis of a kinematical model for a 3-D rotating wind from an accretion disk. The implicit assumption is that the wind is resonant scattering the disk continuum photons producing the observed line profiles. Here we concentrate on the CIV line of nova-like variable systems for which no eclipse, partial eclipse and full eclipse are observed. A similar study of dwarf novae in outburst is in progress.

CV system parameters, such as primary mass, inclination angle, accretion rates, *etc.*, have large errors due to observational uncertainties and model dependence, and generally differ from observer to observer. Even neglecting observational uncertainties, Wade (1990b) demonstrates that a dispersion of $\sim 20\%$ in the radius of the secondaries of a given mass would lead to an uncertainty in the secondary mass of 30% and a 5–45% uncertaintly in the white dwarf primary mass. In view of all this, we have defined generic models for each object (see Table II), basing the white dwarf mass and radius on the average values used in the literature. The other parameters were determined on the basis of a parameter study with the aim of obtaining the best possible fit to selected *IUE* low resolution spectra. We find that a unique solution for the wind mass loss rate is not possible unless the accretion rate is also specified. As the distances to individual CVs are poorly known, there are large uncertainties in the accretion rates given by equation (1). We have therefore chosen to present results for two values for $\dot{M}_a$ for each system in order to demonstrate how the mass loss rate required to produce the observed spectra varies with $\dot{M}_a$. The pair of solutions for

each CV are referred to as the low and high accretion cases which also correspond to low and high mass loss rates and to the wind flow originating in the disk close to and far from the white dwarf. A dynamical model for a 2-D disk wind should remove this uncertainty in model parameters. In the spectral fitting we have scaled our model spectral intensities to the observed intensities and do not attempt to compare absolute values. We also assume in our generic models that the BL has little effect on the ionization balance in the wind due to the large optical depth. The effects of varying T_{BL} are discussed below.

(a) *RW Sextantis*

RW Sex is a non-eclipsing system with strong P Cygni profiles evident in its spectra. In spectral fitting we held fixed the white dwarf mass and radius and varied all other parameters. The *IUE* spectra for RW Sex show considerable variation in both the continuum intensity and in the CIV line profile. This is presumably due to fluctuations in the accretion and mass loss rates. While these variations were not large, we felt that spectral fitting with the aim of producing a mean synthetic spectrum would be misleading. We limited ourselves here to presenting a representative analysis of the spectrum SWP 22705.

In Figure 2 we show the synthetic CIV lines calculated for our generic models (Table IIa) superimposed on the SWP 22705. The *IUE* spectrum was shifted -2Å to align the emission peak. The synthetic line models do not take into account variations in the continuum intensity with frequency. To fit observations, the model spectra are first scaled to the *IUE* continuum in the red wing. A small linear term is then added to adjust the synthetic line to match the blue wing continuum. We find that both emission and absorption parts of the synthetic lines are in good agreement with the *IUE* spectrum. It is important to note that our models require mass loss rates for the low and high accretion rate cases that are respectively only 4% and 13% of the accretion rate. The increased fractional value for $\dot{M}_w$ for the high accretion case comes about because for this case the wind is initiated from a larger area of the disk. Both model winds are initially very optically thick to the CIV line, with the local angle averaged Sobolev escape probability, $< (1 - e^{-\tau_S})/\tau_S >$,

much less than unity. The escape probability increases to 1/2 at a distance $\simeq 70R_{WD}$ from the white dwarf for both accretion cases. This occurs well before terminal velocity is reached. The rapid drop off in optical depth beyond this point is due the decrease in the wind of both the density and the ground state ionization fraction of CIV, ξ. The model line spectrum is not sensitive to changes is local density or ionization state in regions of the wind which are optically thick. As is shown in Figure 3, ξ is $<<$ 1 very close to the disk, peaks at the value $\simeq$ 70% and decreases again at large distance. The peak occurs at a height about the disk of $\simeq 8R_{WD}$ and $\simeq 2R_{WD}$ for the low and high accretion cases respectively. For the low accretion case ξ levels off far from the disk at roughly 30%, while for the high case ξ rapidly decrease with height until the CIV population is negligible. The difference in the ionization profiles for these two cases stems from the larger luminosity for the high accretion case which enhances photoionization in the wind. The increased mass loss for this case comes from a greater initial area, leading to similar densities at the base of the wind. To determine where above the disk the scatter line emission at differing wavelenghts originate we have calculated the emission per unit length in z and plot the resulting contours in Figure 4. This emission does not take into account the reduction of the disk continuum intensity by absorption, but presents solely the emission from the wind. Shadowing effects by the white dwarf and the disk are however included. It is evident from Figure 4 that emission near the line center at 1550Å comes from a very extended region extending $\simeq 100R_{WD}$ above and below the disk. The red and blue emission wings originate from regions with much narrower width in z and a greater height above and below the disk.

As is shown in Paper II, the introduction of rotation in the wind strongly modifies the resonant velocity surfaces and introduces a radial shear in the velocity which decreases the Sobolev optical depth. This result in a reduction in line center intensity and the broadening of the emission component of the line. Rotation also introduces of a potentially observable *redshifted* absorption from the material above the disk. This redshifted absorption results

from part of the wind that is rotating away from the observer, but is still seen projected against the disk surface. Comparisons between our disk wind synthetic line and that for a purely *spherical* outflow from the surface of the WD were made. Good fits to the SWP 22705 spectrum were obtained for both the low and high accretion rates cases, but the spherical mass loss rate required was three times larger than that found for the disk winds. For the high accretion case, this required that the mass loss rate be 45% of the accretion rate. Use of a radial wind with the density decreased by a positive power of $\cos\theta$ (*e.g.* Drew 1987), would lead to the necessity of an even larger value for $\dot{M}_w$ to produce the observed absorption profile.

Our choice of the inclination angles for the disk wind model spectra is evident from Figure 5, which shows model line intensities as a function of i. The absorption component of the synthetic line is weakly dependent upon i as long as the observer views the disk through the wind (*i.e.* $i < \theta_{max}$). The ratio of the emission component to the continuum is strongly dependent upon i. As these spectra are scaled to the continuum intensity, this variation in the emission peak to continuum intensity is due mainly to variations in the continuum intensity caused by limb darkening and the cos i dependence of the observed surface area of the disk. The best fits were achieved for $i = 59^o$ and $i = 62^o$ for the low and high accretion rate cases respectively. These values are somewhat higher than the range given by Bolick *et al.* (1987). The effects of varying $\dot{M}_a$ (Figure 6) and $\dot{M}_w$ (Figure 7) on the line shape (and holding all other parameters fixed) are evident in changes in both the absorption profile and the emission feature. Variations in the accretion rate affect the wind directly by altering the ionizing flux and indirectly by modifying the disk temperature which determines where on the disk the wind originates. Increasing the accretion rate, and hence the continuum UV intensity, tends to over ionize the wind decreasing ξ, and affects the spectra in a manner similar to reducing the $\dot{M}_w$. Increasing the accretion rate generally leads to reduced absorption and emission in the line profile. Enhanced absorption is not evident for the low accretion rate case at decreased accretion because the reduction in

the outer radius of the wind with $\dot{M}_a$ (which for this case is comparable with scale of the disk emitting region) leads to a significant decrease in the obstruction of the disk emitting region by the wind. Changing the mass loss rate modifies the density in the wind which in turn also affects the ionization balance. The depth and wavelength dispacement from line center of the absorption minimum are rapidly increasing functions of $\dot{M}_w$. The emission feature maximum and its red wing also increase with $\dot{M}_w$.

The temperature of the BL is a matter of controversy. It is expected that if the white dwarf is not rotating close to breakup, then nearly half of the total gravitational potential generated by the accreting matter should be released as radiation in the boundary layer (Lynden-Bell & Pringle 1974). Pringle (1977) and Pringle & Savonije (1979) predicted that for accretion rates typical of nova-line variables and dwarf novae in outburst the value of T_{BL} should be in the range 200,000–500,000 °K. Such high values for T_{BL} play havoc with synthetic line modeling by highly over ionizing the wind unless the mass loss rate is unreasonable high (see, *e.g.*, Mauche & Raymond 1987). For our generic RW Sex models, values of the boundary layer temperatures $\lesssim$ 60,000 °K and $\lesssim$ 80,000 °K for the low and high accretion rate models respectively did not significantly modify the predicted spectra. Higher BL temperatures require increases in the mass loss rate to prevent the wind from becoming overionized and too optically thin. The low values for T_{BL} $\lesssim$ 60,000–80,000 °K for our generic models are consistent with the recent study of BL temperatures by Hoare and Drew (1991) who conclude that typical BL temperatures should range between 50,000–100,000 °K. Observations of soft X-ray fluxes and ionization state of CV winds point to a lower T_{BL} than the one predicted theoretically, as well. Other explanations, such as interstellar and/or photoelectric absorption are also viable (*e.g.* Raymond and Mauche 1991).

(b) *RW Triangulis*

This nova-like eclipsing variable is seen at large inclination angle. The CIV line is observed only in emission with no absorption component. Figure 8 gives our generic

model spectra superimposed on the four SWP images for CIV line. The emission peak of the synthetic spectra are scaled to the intensity 3×10^{-13} erg cm^{-2} s^{-1}Å^{-1} and no modification was made to adjust to the observed continuum in either red or blue wings. The *IUE* spectra SWP 16041, SWP 16063, and SWP 17621 were shifted by -1Å, while SWP 16064 was shifted -3Å to align the emission peaks. These *IUE* spectra were taken when the system was not eclipsing and are in good agreement with each other. In fitting RW Tri, as compared with RW Sex, we find that we have a greater degree of freedom as our only contraint from absorption is that it must not produce a significant feature. The model synthetic line profiles produced are in good agreement with the *IUE* spectra. The observed spectra, however, show more asymmetry than is predicted from the model spectra. Our generic disk wind models for RW Tri remains optically thick over nearly all of the acceleration region of the wind, with the averaged local escape probability raising to 1/2 at $\simeq$ 60–70 R_{WD} close to where the terminal velocity is reached. The ionization structure of the CIV ground state, ξ, shown in Figure 9 in similar to that for RW Sex, with the ionization peaks now at a height of $\simeq 25R_{WD}$ and $\simeq 2RWD$ above the disk for the low and high accretion cases respectively. For the low accretion case ξ again levels off to a near constant value at large distance (with $\xi \simeq 0.6$). The spatial extent of the observed scattered line emission above the disk is shown in Figure 10. For our RW Tri models, emission both at line center and in the red and blue wings comes from a region which extends roughly 100 R_{WD} above and below the disk.

For RW Tri synthetic spectral lines calculated using a spherical model did not lead to acceptable line profiles. We found that mass loss rates which reproduced the observed emission line to continuum ratio and the observed line width lead to an appreciable blue shifted absorption feature. The absorption disappears at large inclination angles, but requires such low mass loss rates to retain the emission to continuum ratio that the wind becomes highly optically thin early, well before reaching terminal velocity. This results in an emission line profile of roughly half the width of that observed. Increasing the

terminal velocity does not help broaden the line as this leads to even lower densities and less scattering in the outer region of the wind. The spherical wind fit to RW Tri by Mauche and Raymond (1987) relied on a constant ionization fraction for the CIV ground state in the wind. In our model we find that this is not a valid assumption for conditions which do not produce appreciable absorption profiles. Significant absorption does not occur for the disk winds since the inclination angle to the observer for the RW Tri models is greater than the maximum angle for the disk wind streamlines, θ_{max}. For a radial wind, the absoprtion could be reduced by using a mass loss rate which decreases as a function of angle θ, as was suggested by Drew (1987). The need to reduce the density at large angles for a radial flow model in RW Tri however is opposite to what is needed for a radial model for RW Sex, where enhanced absorption for a given total mass loss rate is desirable to lessen the ratio of $\dot{M}_w / \dot{M}_a$.

Variations in our RW Tri model spectrum with respect to inclination angle are shown in Figure 11. As the peak intensity is scaled to a fixed value, varying i modifies the continuum intensity and the line width only. We find that the absolute value of the emission peak varies very quite slowly with i, so that it is the continuum intensity which primarily varies with the inclination angle. Too low or too high a value for i leads to a model continuum which is respectively higher or lower than the *IUE* observations. For large inclinations, details of the disk vertical structure and limb darkening may have a significant affect on i, but such details are beyond the scope of this paper. As the wind is quite optically thick, and without absorption structure, increasing the mass loss rate does not lead to a significant change in the line profile (see Figure 12). Decreases in $\dot{M}_w$ are more appreciable, as this leads to the wind becoming increasingly optically thin, reducing the ratio of the line emission peak to the continuum. The sensitivity of changing the accretion rate is show in Figure 13. As expected, increasing $\dot{M}_a$, which increases the UV flux and therefore leads to a reduction in the wind optical depth, has a greater effect of the line profile than does decreasing $\dot{M}_a$.

The effect of the BL on the RW Tri model spectra is similar to that for the RW Sex case. Values of the boundary layer temperatures $\lesssim 60,000$ °K and $\lesssim 90,000$ °K for the low and high accretion rate models respectively did not significantly modify the predicted spectra. Again, higher BL temperatures can be accommodated if the mass loss rate is correspondingly increased.

(c) V Sagittae

As in the case of RW Tri, V Sge is seen at large inclination (close to 90°), and has no observed absorption profile associated with in its UV lines. Most large inclination nova-like variables have gaussian profiles with widths $\sim 5 \pm 1$Å (Mauche, Córdova and Verbunt 1988). Figure 14 shows our generic model spectra for CIV and two representative *IUE* SWP images. The SWP spectra have been shifted by -2.8Å to align their emission peaks. For this system we have assumed an inclination angle of 90°. As our disk model is assumed to be flat we are unable to accurately determine the continuum intensity. The model spectra were therefore scaled to mean peak intensity of SWP 25604 and SWP 25606, with a constant continuum intensity added. As the emission peak to continuum ratio is thus prescribed, model parameters for the fitted spectra of V Sge are even less constrained than is the case for RW Tri. Because V Sge appears to be intrinsically brighter than RW Sex or RW Tri we have chosen $\dot{M}_a$ for our V Sge low accretion rate case to be comperable with $\dot{M}_a$ for the RW Sex and RW Tri high accretion rate cases. The high accretion rate case for V Sge uses a value for $\dot{M}_a$ which is a factor of ten larger than the low accretion case. The mass loss rates were chosen to correspond to winds which became optically thin just prior to reaching terminal velocity. The ratio of mass loss to accretion rate are 5% and 10% for the low accretion rate and high accretion rate cases. Figure 15 shows the ionization structure in the wind of the CIV ground state. As it was seen already in the models for RW Sex and RW Tri, the peak ionization fraction for our V Sge models occurs closer to the disk for larger accretion rates. The variation in line emission with position above and below the disk is shown in Figure 16. The structure is similar to RW Tri, which

is also seen at high inclination, with strong emission over most of the line width coming from a region exdending over 100 R_{WD} from the disk.

Because of the very high mass loss rate the model spectra for V Sge were found to be insensitive to the boundary layer for up to $T_{BL} \sim 150{,}000$ °K. This is due in part to the fact that, because of our scaling, we are primarily comparing synthetic to observed line widths and not features such a the emission to continuum ratio. The absolute disk wind emission intensities were found to vary little for $T_{BL} \lesssim 100{,}000$ °K. We similarly find that changes in the mass loss rate or the accretion rate by factors of two upwards or downwards did not significantly affect the model line spectrum. As a spherical wind shows no disk obscuration at 90° inclination we were able to fit the observed spectra for this type outflow with the disk wind values for $\dot{M}_a$ and $\dot{M}_w$. Clearly further constraint must be applied from either eclipse observations or theoretical wind modeling in order to determine conditions for the V Sge system.

6. Conclusions

In this work we have compared the observed UV line profiles from three nova-like variables to the synthetic lines calculated on the basis of a 3-D kinematical wind model from an accretion disk. We have demonstrated that taking into account the observed dispersion in primary masses, inclination angles and accretion rates in these systems, good fits can be obtained. We find that, based on our kinematical model, disk winds can reproduce the observed line profiles from CVs, which include the P Cygni profiles at low inclination and pure emission lines at large inclination without invoking additional assumptions. In particular, the minimum of the absorption profile residual flux occurs close to the line center, typically blue-shifted by few hundred km s^{-1}. The best line fits were obtained by using a power law profile with acceleration slightly faster than linear and with the wind acceleration scale height $R_v >> R_{WD}$. We note in passing that the WD radius is actually a poor measure of the wind acceleration scale height. This follows from

the fact that the size of the disk emission region, which produces the photons that are photoionize and resonantly scattered in the wind, and the extent over which the wind is initiated on the disk are significantly greater than the WD radius.

A self-consistent photoionization model for the wind allows us to identify and to accurately map the resonant scattering regions above the disk. We find that for a broad range of disk wind parameters the scattering region extends $\sim R_v$ above the disk plane and has a strongly bi-conical character due to the wind being confined between angles θ_{min} and θ_{max}.

Disk winds are preferable to spherical winds which originate on the WD for several reasons. First, we find that they require a much lower ratio of $\dot{M}_w / \dot{M}_a$ for systems which show P Cygni profiles, such as RW Sex, making them more plausible on the energy grounds, especially if the winds are driven by radiation pressure. For high inclination systems, such as RW Tri, the absence of an observed absorption profile leads for spherical winds to the necessity of such a low mass loss rate that the wind becomes very optically thin before reaching terminal velocity and the resulting emission line is too narrow to fit the observed profiles. Much of this drop in the optical depth comes from a decrease in the fractional ionization in the CIV ground state as the density decreases in the accelerating wind. The assumption of constant ionization which has been used for radial winds in the literature overestimates the line emission in the red and blue wings of the emission line. Second, for disk winds matter is channeled into extended bi-conical emission regions above and below the disk which reflect the overall distribution of mass in the wind irregardless of detailed assumptions about the velocity field or limb darkening. This naturally explains why the UV lines do not experience eclipses as much as the continuum does and why high inclination CVs do not show absorption features. Third, the rotation in the wind introduces a radial shear in the velocity field which decrease the resonance line optical depth and reduce the line center intensity. In high-inclination systems it will produce rotationally enhanced broadening of the lines. This effect should be observable with the

high-resolution instruments.

Rotation is also responsible for some amount of a redshifted absorption which is potentially observable in the low-to-intermediate inclination systems. It is produced by the part of the wind which is rotating away from the observer and is seen projected onto a disk. While such absorption may be observed only when line emission is weak, it appears to be a salient property of the disk wind.

We find that a unique fit to the observed profiles is not possible on the basis of kinematical model alone. However, a dynamical model for a 2-D outflow from a disk should remove this limitation.

ACKNOWLEDGEMENTS.

We have benefitted from numerous discussions with our collegues Juhan Frank, Chris Mauche and John Raymond. Special thanks go to Chris Mauche for his constant patience and willingness to clarify observational 'mysteries'. We also are grateful to the RDAF staff in Boulder (which is funded under NASA contract NAS5-28731) and especially Gregg Ellison for the technical assistance. This work was performed under the auspices of the US Department of Energy by LLNL user contract number W-7405-ENG-48 and supported in part by NASA grant NAG5-1387.

REFERENCES

Abbott, D.C. *Astrophys. J.* **259**, 282 (1982).

Bailey, L. *Mon. Not. R. Astr. Soc.* **197**, 31 (1981).

Boggess, A. *et al. Nature* **275**, 372 (1978).

Bolick, U., Beuermann, K., Bruch, A. & Lenzen, R., in Proc. *IAU* Coll. No. 93 (*Astrophys. Sp. Sci.* **130**, 175 [1987]), ed. Drechsel *et al* .

Cannizzo, J.K. & Pudritz, R.E. *Astrophys. J.* **327**, 840 (1988).

Cassatella, A., Barbero, J. & Benvenuti, P. *Astron. Astrophys.* **144**, 335 (1985).

Córdova, F.A. (1986) in *The Physics of Accretion onto Compact Objects,* eds. K.O.Mason *et al.* (Springer-Verlag: Heidelberg), p. 339.

Córdova, F.A. & Howarth, I.D. (1987) in *Scientific Accomplishments of the IUE,* ed. Y.Kondo (Dordrecht: Reidel), p. 467.

Córdova, F.A. & Mason, K.O. *Astrophys. J.* **260**, 716 (1982).

Córdova, F.A. & Mason, K.O. *Astrophys. J.* **290**, 671 (1985).

Drew, J. *Mon. Not. R. Astr. Soc.* **224**, 595 (1987).

Drew, J. (1991) in Proc. *IAU* Coll. 122 on *Physics of Classical Novae*, eds. A.Cassatella & R.Viotti (Springer-Verlag: Heidelberg), p. 228.

Drew, J. & Verbunt, F. *Mon. Not. R. Astr. Soc.* **213**, 191 (1985).

Drew, J., Hoare, M.G. & Woods, J.A. *Mon. Not. R. Astr. Soc.* **250**, 144 (1991).

Emmering, R.T., Blandford, R.D. & Shlosman, I. *Astrophys. J.* **385**, 460 (1992).

Frank, J. & King, A.R. *Mon. Not. R. Astr. Soc.* **195**, 227 (1981).

Frank, J., King, A.R., Sherrington, A.R., Jameson, R.F. & Axon, D.J. *Mon. Not. R. Astr. Soc.* **195**, 505 (1981).

Greenstein, J.L. & Oke, J.B. *Astrophys. J.* **258**, 209 (1982).

Guinan, E.F. & Sion, E.M. *Astrophys. J.* **258**, 217 (1982).

Hamada, T. & Salpeter, E.E. *Astrophys. J.* **134**, 683 (1961).

Herbig, G.H., Preston, G.W., Smak, J. & Paczyński, B. *Astrophys. J.* **141**, 617 (1965).

Honeycutt, R.K., Schlegel, E.M. & Kaitchuck, R.H. *Astrophys. J.* **302**, 388 (1986).

Horne, K. (1983) Ph. D. thesis, California Institute of Technology.

Horne, K. & Stiening, R.F. *Mon. Not. R. Astr. Soc.* **216**, 933 (1985).

Hoare, M.G. & Drew, J.E. *Mon. Not. R. Astr. Soc.* **249**, 452 (1991).

Kaitchuck, R.H., Honeycutt, R.K. & Schlegel, E.M. *Astrophys. J.* **267**, 239 (1983).

Kallman, T.R. *Astrophys. J.* **272**, 238 (1983).

Kallman, T.R. & Jensen, K.A. *Astrophys. J.* **299**, 277 (1985).

King, A.R., Frank, J., Jameson, R.F. & Sherrington, M.R. *Mon. Not. R. Astr. Soc.* **203**, 677 (1983).

Klare, G., Krautter, J., Wolf, B., Stahl, O., Vogt, N., Wargau, W., & Rahe, J. *Astron. Astrophys.* **113**, 76 (1982).

Koch, R.H., Corcoran, M.F.,, Holenstein, B.D. & McCluskey, G.E.Jr. *Astrophys. J.* **306**, 618 (1986).

Krautter, J., Klare, G., Wolf, B., Duerbeck, H.W., Rahe, J., Vogt, N. & Wargau, W. *Astron. Astrophys.* **102**, 337 (1981).

LaDous, C. *Sp. Sci. Rev.* **52**, 203 (1990).

Lynden-Bell, D. & Pringle, J.E. *Mon. Not. R. Astr. Soc.* **168**, 603 (1974).

Marsh, T.R. & Horne, K. *Astrophys. J.* **349**, 593 (1990).

Mauche, C.W. & Raymond, J.C. *Astrophys. J.* **323**, 690 (1987).

Mauche, C.W., Córdova, F.A. & Verbunt, F. *BAAS***20**, 1020 (1988).

Naylor, T., *et al.* *Mon. Not. R. Astr. Soc.* **231**, 237 (1988).

Patterson, J. *Astrophys. J. Supp. Ser.* **54**, 443 (1984).

Patterson, J. & Raymond, J.C. *Astrophys. J.* **292**, 550 (1985).

Polidan, R.S., Mauche, C.W. & Wade, R.A. *Astrophys. J.* **356**, 211 (1990).

Pringle, J.E. *Mon. Not. R. Astr. Soc.* **178**, 195 (1977).

Pringle, J.E. & Savonije, G.J. *Mon. Not. R. Astr. Soc.* **187**, 777 (1979).

Pudritz, R.E. & Norman, C.A. *Astrophys. J.* **301**, 571 (1986).

Raymond, J.C. & Mauche, C.W. (1991) in *Extreme UV Astronomy*, ed. R.F.Malina & S.Bowyer (New-York: Pergamon Press), p. 163.

Ritter, H. *Astron. Astrophys. Suppl. Ser.* **85**, 1179 (1990).

Rybicki, G.B. & Hummer, D.G. *Astrophys. J.* **219**, 654 (1978).

Rybicki, G.B. & Hummer, D.G. *Astrophys. J.* **274**, 380 (1983).

Shakura N.I. & Sunyaev, R.A. *Astron. Astrophys.* **24**, 337 (1973).

Shlosman, I. & Vitello, P.A.J. *Astrophys. J.* , in preparation, Paper II.

Sobolev, V.V. *Sov. Astron.-AJ* **1**, 678 (1957)

Verbunt, F. *Astron. Astrophys. Suppl. Ser.* **71**, 339 (1987).

Vitello, P.A.J. & Shlosman, I. *Astrophys. J.* **327**, 680 (1988), Paper I.

Wade, R.A. *Mon. Not. R. Astr. Soc.* **208**, 381 (1984).

Wade, R.A. *Astrophys. J.* **335**, 394 (1990).

Wade, R.A. (1990) in Proc. 11th North American Conf. on CVs and Low Mass X-Ray Binaries *Accretion-Powered Compact Binaries,* ed. C.W.Mauche (Cambridge Univ. Press), p. 181.

Wamsteker, W. *Astron. Astrophys. Suppl. Ser.* **79**, 1 (1989).

Warner, B. *Mon. Not. R. Astr. Soc.* **227**, 23 (1987).

Webbink, R.F. (1990) in Proc. 11th North American Conf. on CVs and Low Mass X-Ray Binaries *Accretion-Powered Compact Binaries,* ed. C.W.Mauche (Cambridge Univ. Press), p. 177.

Williams, G.A., King, A.R., Uomoto, A.K. and Hiltner, W.A. *Mon. Not. R. Astr. Soc.* **219**, 809 (1986).

Withbroe, G.L. (1971) in *The Menzel Symposium of Solar Physics, Atomic Spectra and Gaseous Nebulae,* ed. K.B.Gebbie (Washington: NBS SP-353), p. 127.

Young, P. & Schneider, D.P. *Astrophys. J.* **247**, 960 (1981).

Figure Captions

Fig. 1. Geometry for the disk wind model.

Fig. 2. Synthetic CIV lines for our models of RW Sex (Table IIa) superimposed on SWP 22705.

Fig. 3. Ionization contours for the ground state of CIV for our low accretion rate (a) and high accretion rate (b) models of RW Sex (Table IIa).

Fig. 4. CIV line emission per unit length in z scaled by its peak value for our low accretion rate (a) and high accretion rate (b) models of RW Sex (Table IIa).

Fig. 5. Inclination angle dependance of synthetic CIV lines for the low accretion rate (a) and high accretion rate (b) RW Sex cases superimposed on SWP 22705.

Fig. 6. Effect of different accretion rates on the CIV lines in RW Sex for the low accretion rate (a) and high accretion rate (b) cases. The low and high accretion rate models were modified by changing only $\dot{M}_a$ with all other parameters held fixed. The accretion rates shown are in units of $M_\odot$ yr^{-1}.

Fig. 7. Effect of different mass loss rates from the surface of an accretion disk on the shape of CIV lines in RW Sex for our low accretion rate (a) and high accretion rate (b) models. The models were modified by changing only $\dot{M}_w$ with all other parameters being held fixed. The mass loss rates shown are in units of $M_\odot$ yr^{-1}.

Fig. 8. Synthetic CIV lines for our models of RW Sex (Table IIb) superimposed on SWP 16041, SWP 16063, SWP 16064, and SPW 17621.

Fig. 9. Ionization contours for the ground state of CIV for our low accretion rate (a) and high accretion rate (b) models of RW Tri (Table IIb).

Fig. 10. CIV line emission per unit length in z scaled by its peak value for our low accretion rate (a) and high accretion rate (b) models of RW Tri (Table IIb).

Fig. 11. Inclination angle dependance of synthetic CIV lines for our low accretion rate (a) and high accretion rate (b) models of RW Tri superimposed on SWP 16041, SWP 16063, SWP 16064, and SPW 17621.

Fig. 12. Effect of different mass loss rates from the surface of an accretion disk on the shape of CIV lines in RW Tri for our low accretion rate (a) and high accretion rate (b) models. The low and high accretion rate models were modified by changing only $\dot{M}_w$. The mass loss rates shown are in units of $M_\odot$ yr^{-1}.

Fig. 13. Effect of different accretion rates on the CIV lines in RW Tri for our low accretion rate (a) and high accretion rate (b) models. The low and high accretion rate models were modified by changing only $\dot{M}_a$. The accretion rates shown are in units of $M_\odot$ yr^{-1}.

Fig. 14. Synthetic CIV lines for our models of V Sge (Table IIc) superimposed on SWP 25604, and SPW 25606.

Fig. 15. Ionization contours for the ground state of CIV for our low accretion rate (a) and high accretion rate (b) models of V Sge (Table IIc).

Fig. 16. CIV line emission per unit length in z scaled by its peak value for our low accretion rate (a) and high accretion rate (b) models of V Sge (Table IIc).

TABLE I

IUE Archive Data

SYSTEM	IMAGE	HJD-2,440,000	EXPOSURE (min.)	PHASE	OBSERV.
RW Sex	SWP 22705		8	-	
	SWP 22730		6.5	-	
	SWP 26080		6	-	Polidan
	SWP 26313		6	-	Peters
RW Tri	SWP 16041	4,983.776	50	0.22-0.37	Córdova
	SWP 16063	4,987.526	32	0.39-0.44	Córdova
	SWP 16064	4,987.572	72	0.58-0.80	Córdova
	SWP 16065	4,987.674	50	0.03-0.10	Córdova
	SWP 17617		30	0.90-0.96	Córdova
	SWP 17620		20	0.96-0.02	Córdova
	SWP 17621		35	0.18-0.28	Còrdova
V Sge	SWP 01567	3,646.233	17	0.774	Sobieski
	SWP 25602		8	-	Koch
	SWP 25603		6	-	Koch
	SWP 25604		6	-	Koch
	SWP 25606		5	-	Koch

TABLE IIa

Generic Models for RW Sextantis

Model Parameters	Low Accretion Case	High Accretion Case
M_{WD}	0.8 $M_\odot$	0.8 $M_\odot$
R_{WD}	7×10^8 cm	7×10^8 cm
i	59°	62°
T_{WD}	40,000 °K	40,000 °K
$\dot{M}_a$	1.3×10^{-9} $M_\odot\,yr^{-1}$	1.0×10^{-8} $M_\odot\,yr^{-1}$
$\dot{M}_w$	5×10^{-11} $M_\odot\,yr^{-1}$	1.5×10^{-9} $M_\odot\,yr^{-1}$
θ_{min} ; θ_{max}	15°; 70°	20°; 65°
R_d	19 R_{WD}	36 R_{WD}
r_{min} ; r_{max}	1 R_{WD} ; 3 R_{WD}	4 R_{WD} ; 12 R_{WD}
T-range (wind base)	30,000–50,000 °K	20,000–40,000 °K
R_v	100 R_{WD}	100 R_{WD}
v_∞ ; α	1.7 v_{esc}; 1.3	3.3 v_{esc}; 1.5

TABLE IIb

Generic Models for RW Trianguli

Model Parameters	Low Accretion Case	High Accretion Case
M_{WD}	0.6 $M_\odot$	0.6 $M_\odot$
R_{WD}	8×10^8 cm	8×10^8 cm
i	75°	78°
T_{WD}	25,000 °K	25,000 °K
$\dot{M}_a$	2×10^{-9} $M_\odot\,yr^{-1}$	2×10^{-8} $M_\odot\,yr^{-1}$
$\dot{M}_w$	3×10^{-11} $M_\odot\,yr^{-1}$	1×10^{-9} $M_\odot\,yr^{-1}$
θ_{min} ; θ_{max}	10°; 65°	10°; 65°
R_d	17 R_{WD}	42 R_{WD}
r_{min} ; r_{max}	1 R_{WD} ; 3 R_{WD}	4 R_{WD} ; 12 R_{WD}
T-range (wind base)	30,000–50,000 °K	20,000–40,000 °K
R_v	75 R_{WD}	75 R_{WD}
v_∞ ; α	1.2 v_{esc}; 1.5	2.5 v_{esc}; 1.5

TABLE IIc

Generic Model for V Sagittae

Model Parameters	Low Accretion Case	High Accretion Case
M_{WD}	0.7 $M_\odot$	0.7 $M_\odot$
R_{WD}	8×10^8 cm	8×10^8 cm
i	90°	90°
T_{WD}	25,000 °K	25,000 °K
$\dot{M}_a$	1×10^{-8} $M_\odot\,yr^{-1}$	1×10^{-7} $M_\odot\,yr^{-1}$
$\dot{M}_w$	5×10^{-10} $M_\odot\,yr^{-1}$	1×10^{-8} $M_\odot\,yr^{-1}$
$\theta_{min}\,;\theta_{max}$	10°; 65°	10°; 65°
R_d	31 R_{WD}	79 R_{WD}
$r_{min}\,;r_{max}$	2 R_{WD}; 6 R_{WD}	6 R_{WD}; 13 R_{WD}
T-range (wind base)	30,000–50,000 °K	30,000–50,000 °K
R_v	75 R_{WD}	50 R_{WD}
$v_\infty\,;\alpha$	1.0 v_{esc}; 1.5	1.9 v_{esc}; 1.5

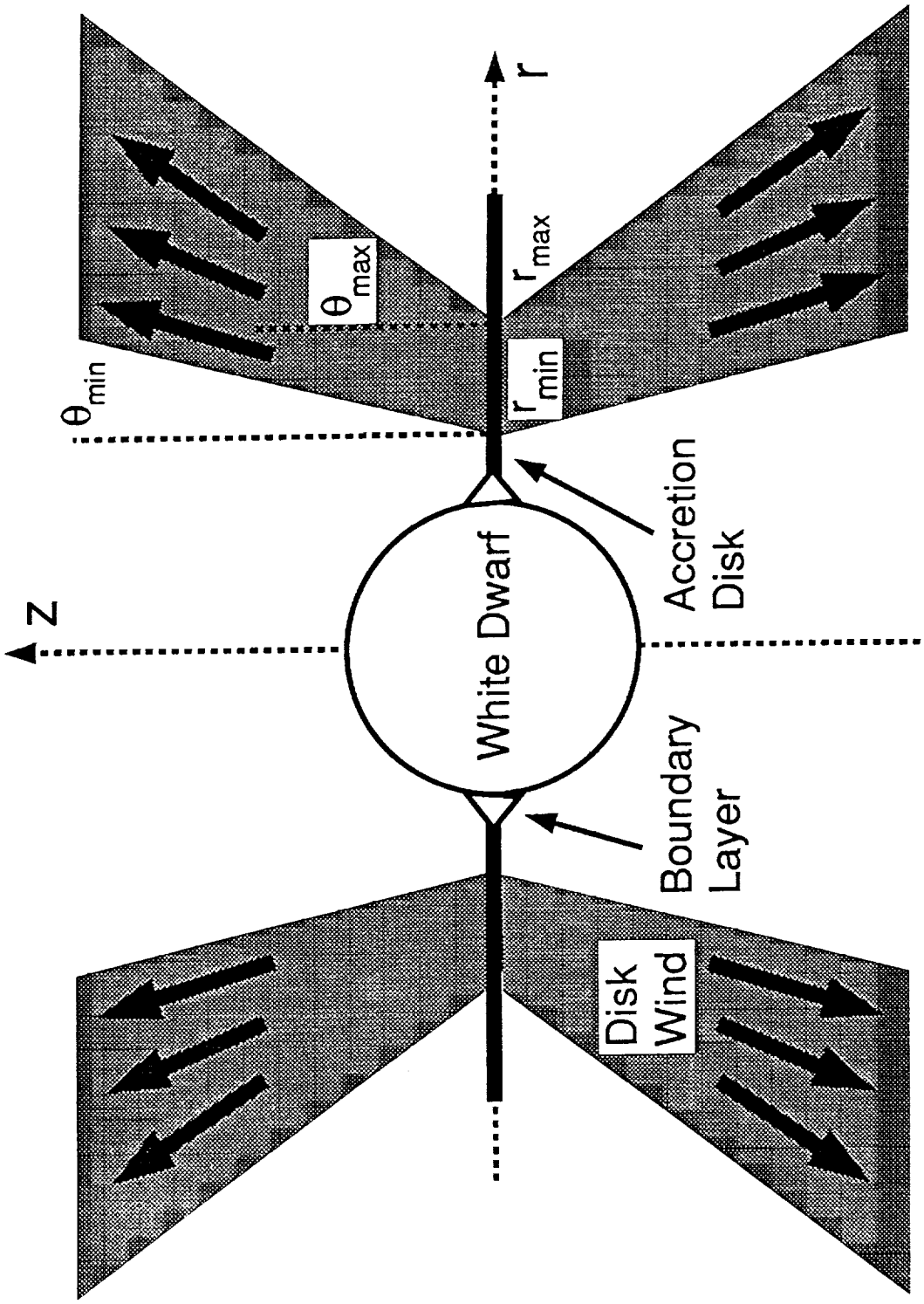
r
r_{max}
θ_{max}
r_{min}
θ_{min}
z
White Dwarf
Accretion Disk
Boundary Layer
Disk Wind

Figure 1

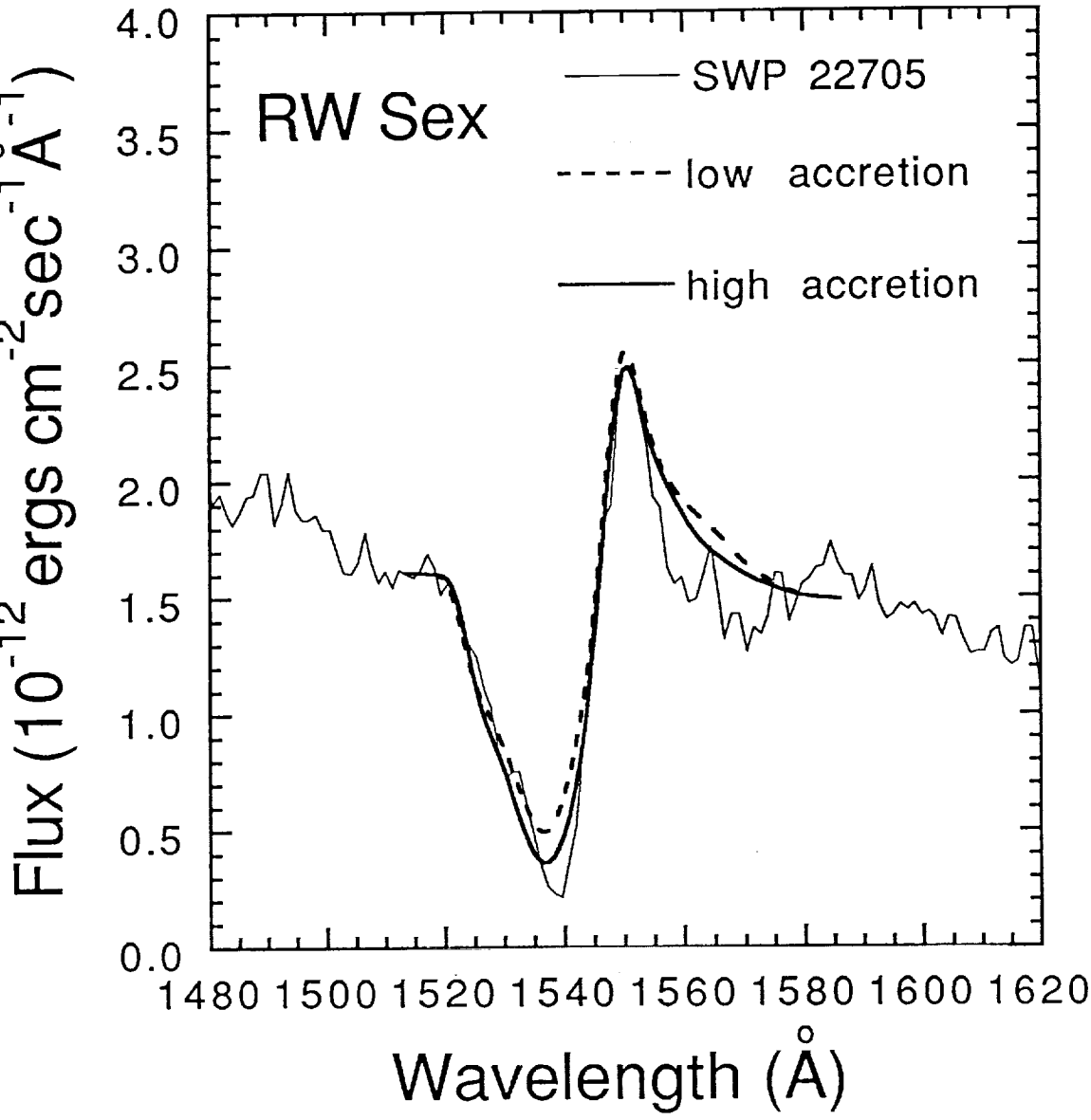
RW Sex
SWP 22705
low accretion
high accretion
Flux (10^{-12} ergs cm^{-2}sec^{-1}Å^{-1})
Wavelength (Å)
4.0
3.5
3.0
2.5
2.0
1.5
1.0
0.5
0.0
1480 1500 1520 1540 1560 1580 1600 1620

Figure. 2

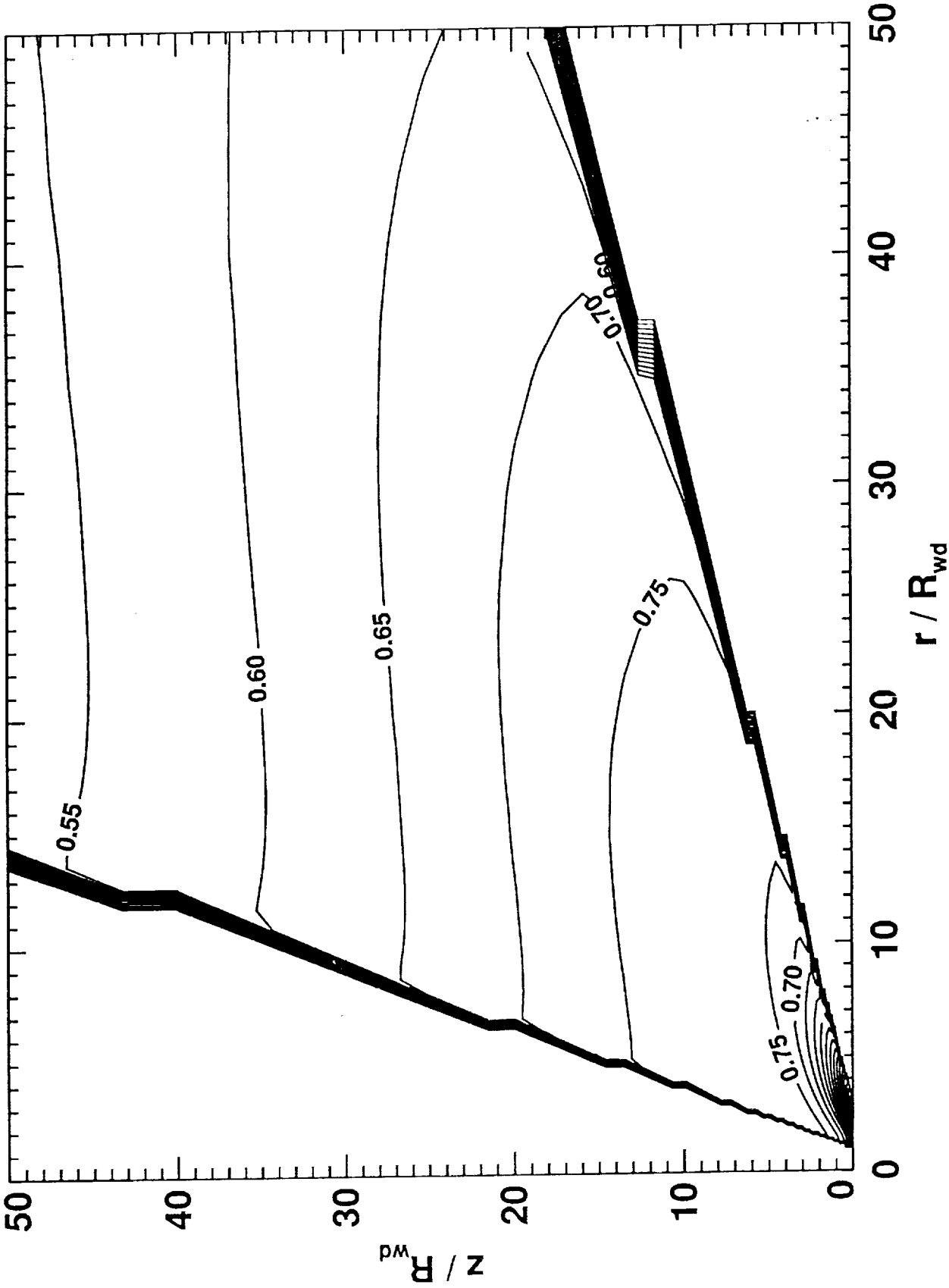

Figure 3a

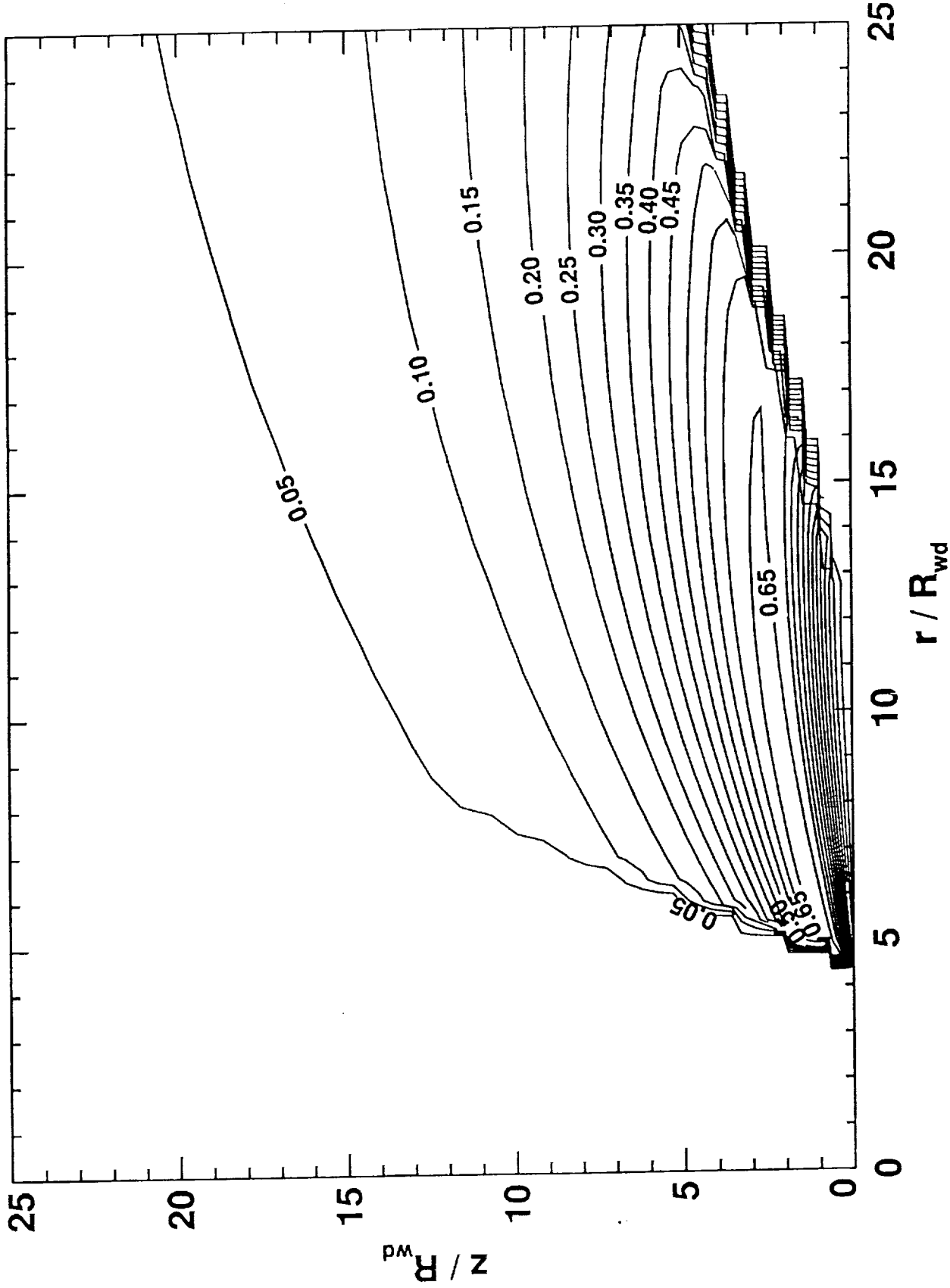

Figure 3b

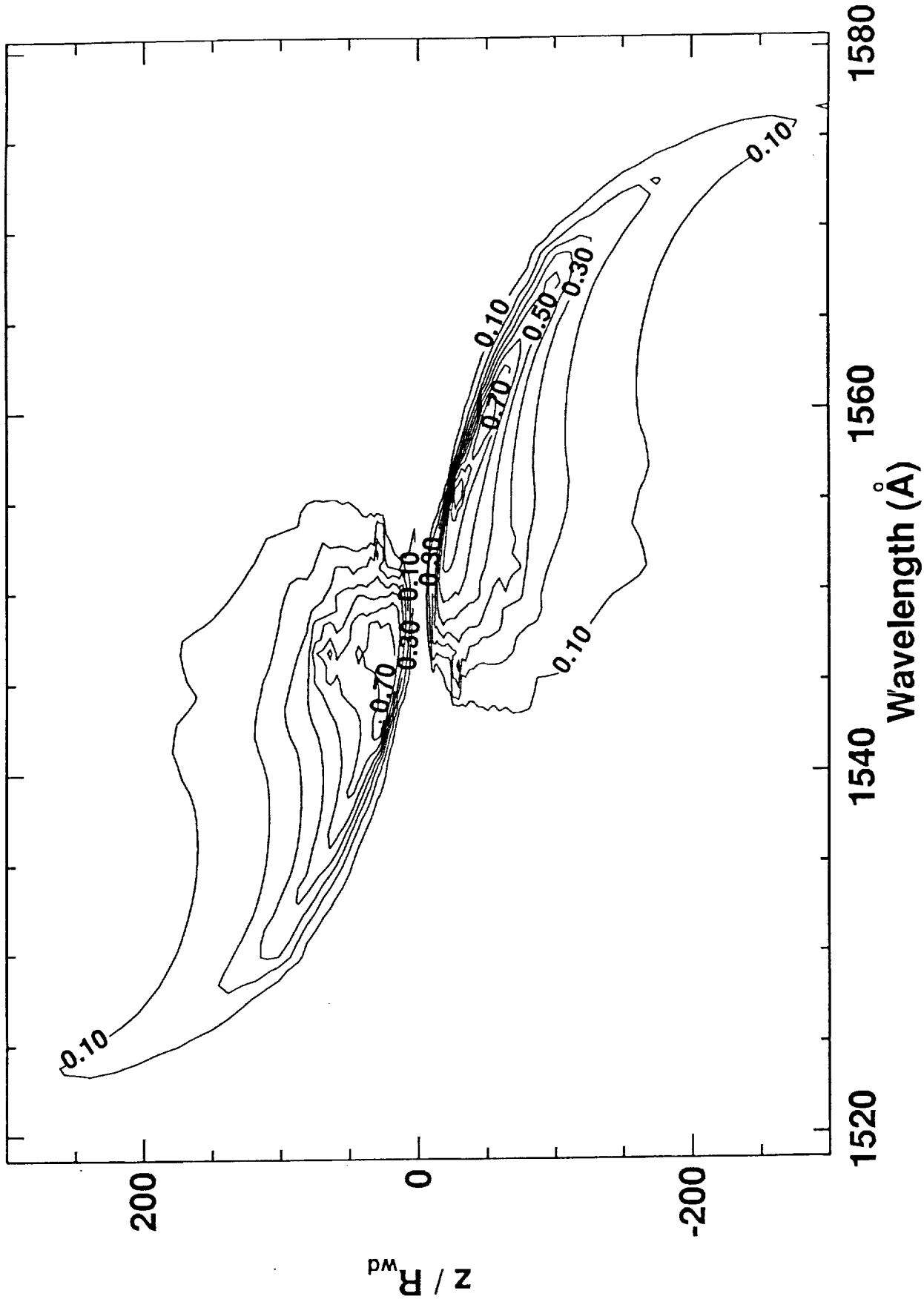
0.10
0.10
0.10
0.10
0.30
0.30
0.30
0.50
0.70
0.70
1520
1540
1560
1580
Wavelength (Å)
200
0
-200
z / R_wd

Figure 4a

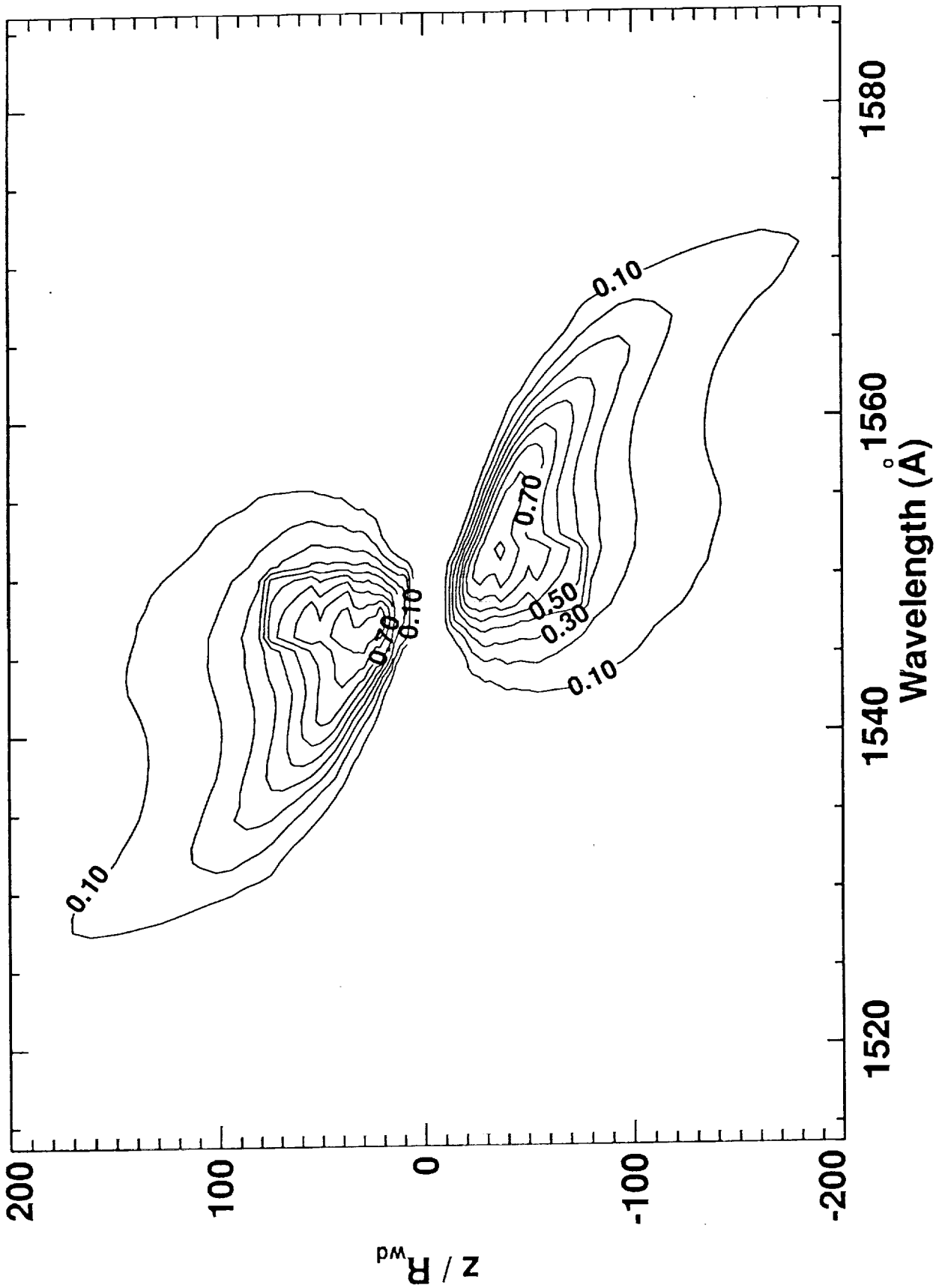
0.10
0.70
0.50
0.30
0.10
0.70
0.10
0.10
200
100
0
-100
-200
1520
1540
1560
1580
Wavelength (Å)
z / R_wd

Figure 4b

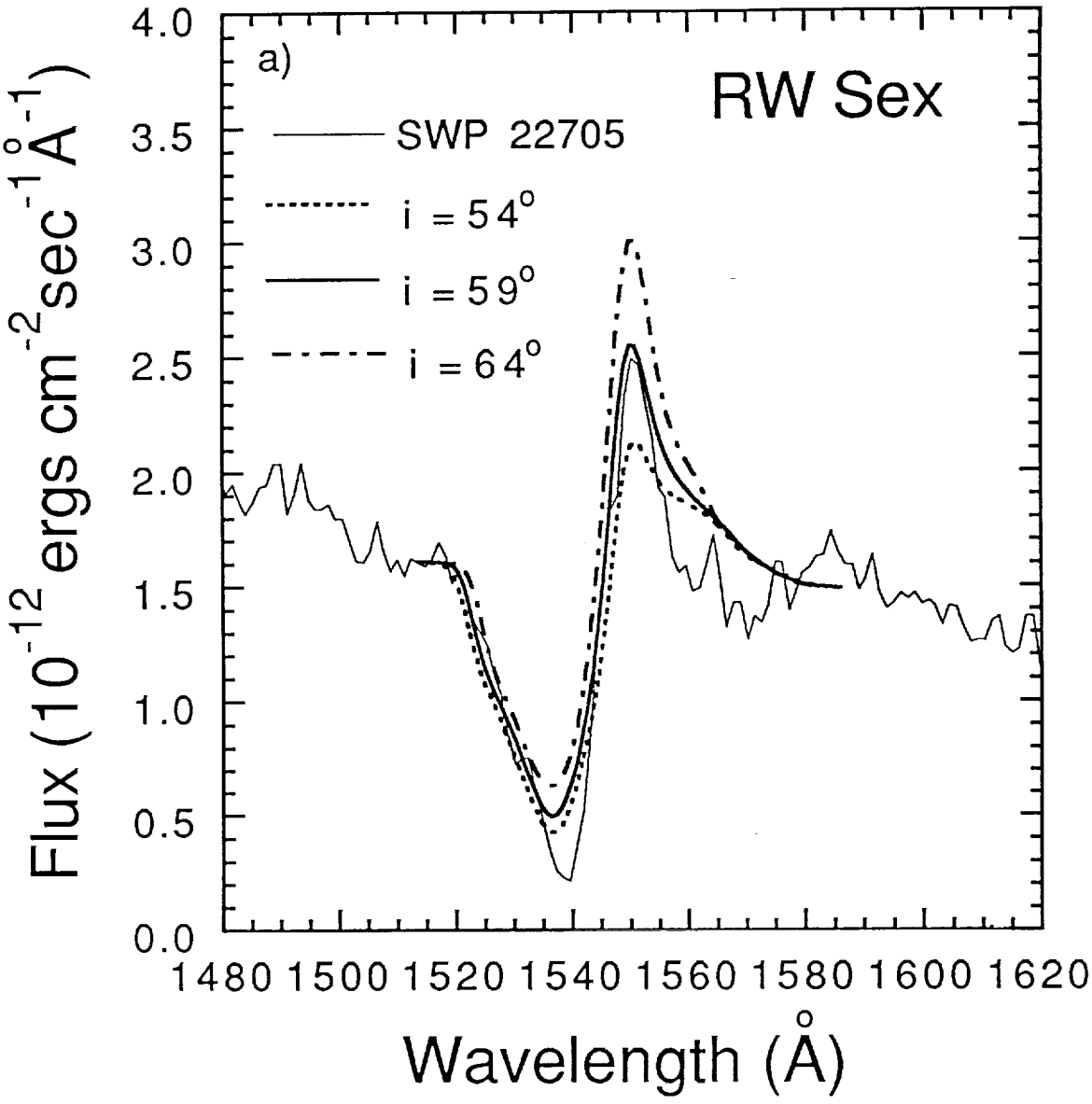
a)
RW Sex
SWP 22705
i = 54°
i = 59°
i = 64°
Flux (10^{-12} ergs cm^{-2}sec^{-1}Å^{-1})
Wavelength (Å)
4.0
3.5
3.0
2.5
2.0
1.5
1.0
0.5
0.0
1480 1500 1520 1540 1560 1580 1600 1620

Figure. 5a

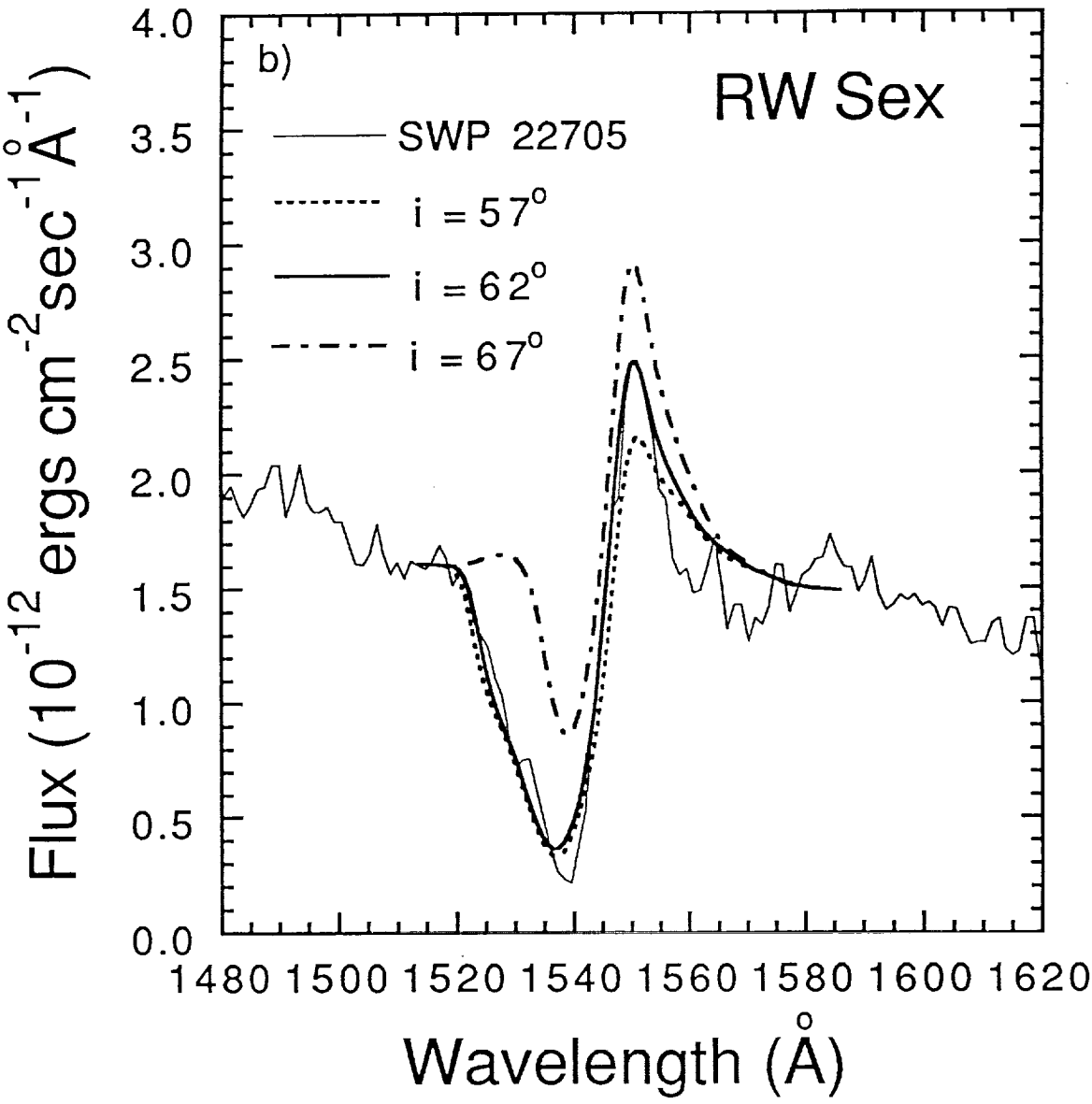
b)
RW Sex
SWP 22705
i = 57°
i = 62°
i = 67°
Flux (10^{-12} ergs cm^{-2}sec^{-1}Å^{-1})
Wavelength (Å)
4.0
3.5
3.0
2.5
2.0
1.5
1.0
0.5
0.0
1480 1500 1520 1540 1560 1580 1600 1620

Figure. 5b

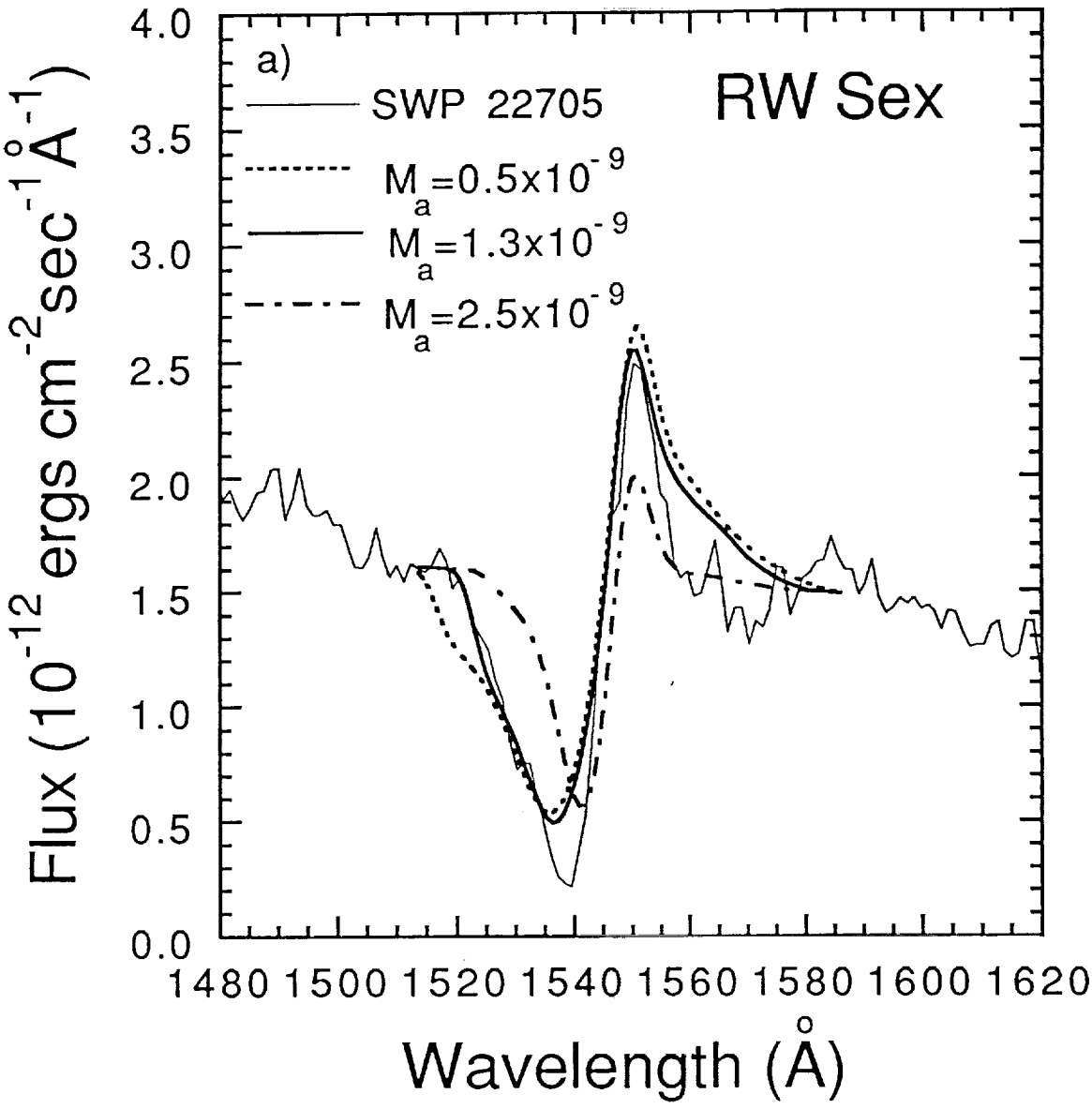
a)
SWP 22705
RW Sex
$M_a=0.5x10^{-9}$
$M_a=1.3x10^{-9}$
$M_a=2.5x10^{-9}$
Flux (10^{-12} ergs cm^{-2}sec^{-1}Å^{-1})
Wavelength (Å)
4.0
3.5
3.0
2.5
2.0
1.5
1.0
0.5
0.0
1480 1500 1520 1540 1560 1580 1600 1620

Figure. 6a

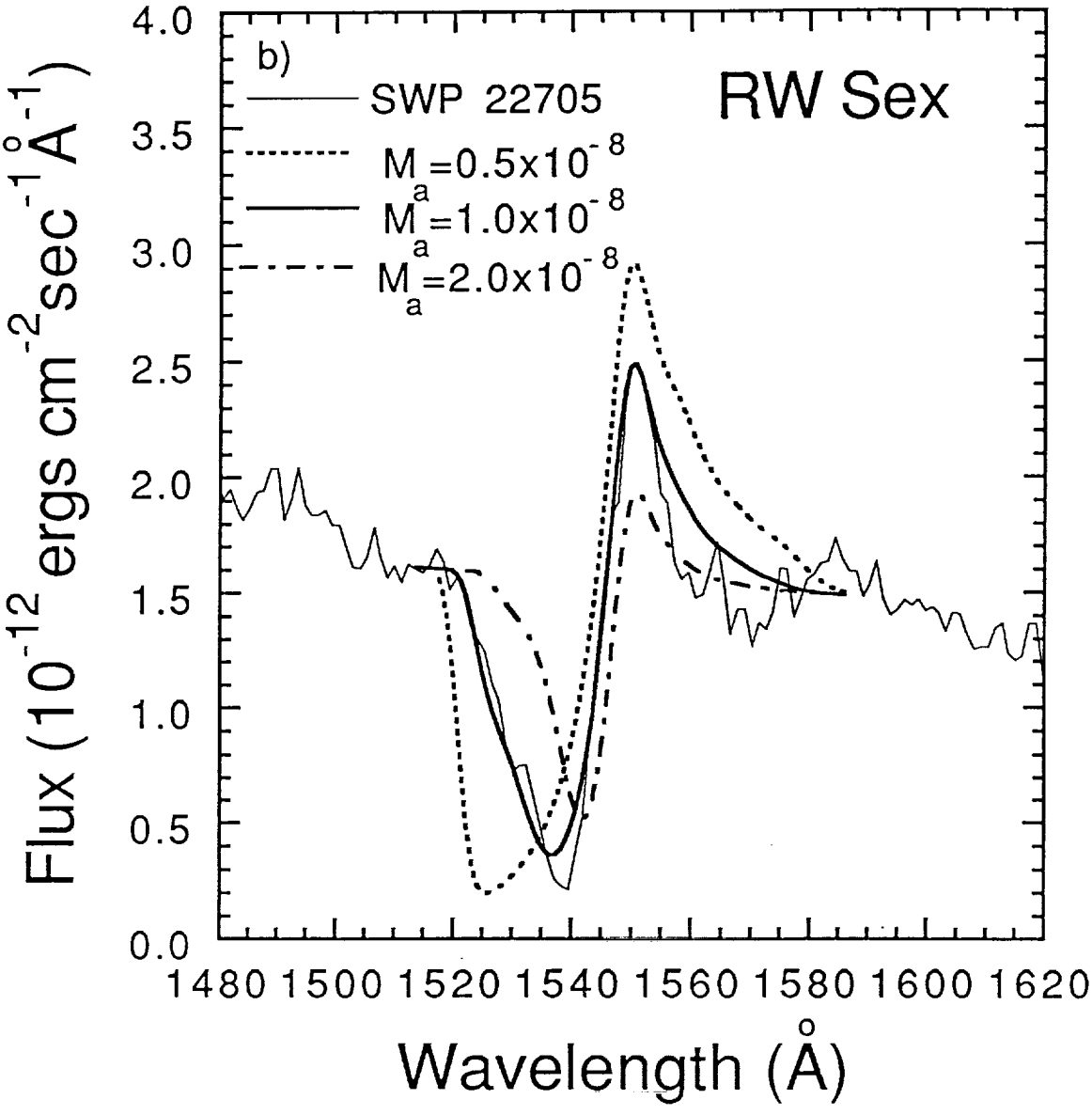
b)
SWP 22705
RW Sex
M =0.5x10^-8
a
M =1.0x10^-8
a
M =2.0x10^-8
a
Flux (10^-12 ergs cm^-2 sec^-1 Å^-1)
Wavelength (Å)
4.0
3.5
3.0
2.5
2.0
1.5
1.0
0.5
0.0
1480 1500 1520 1540 1560 1580 1600 1620

Figure. 6b

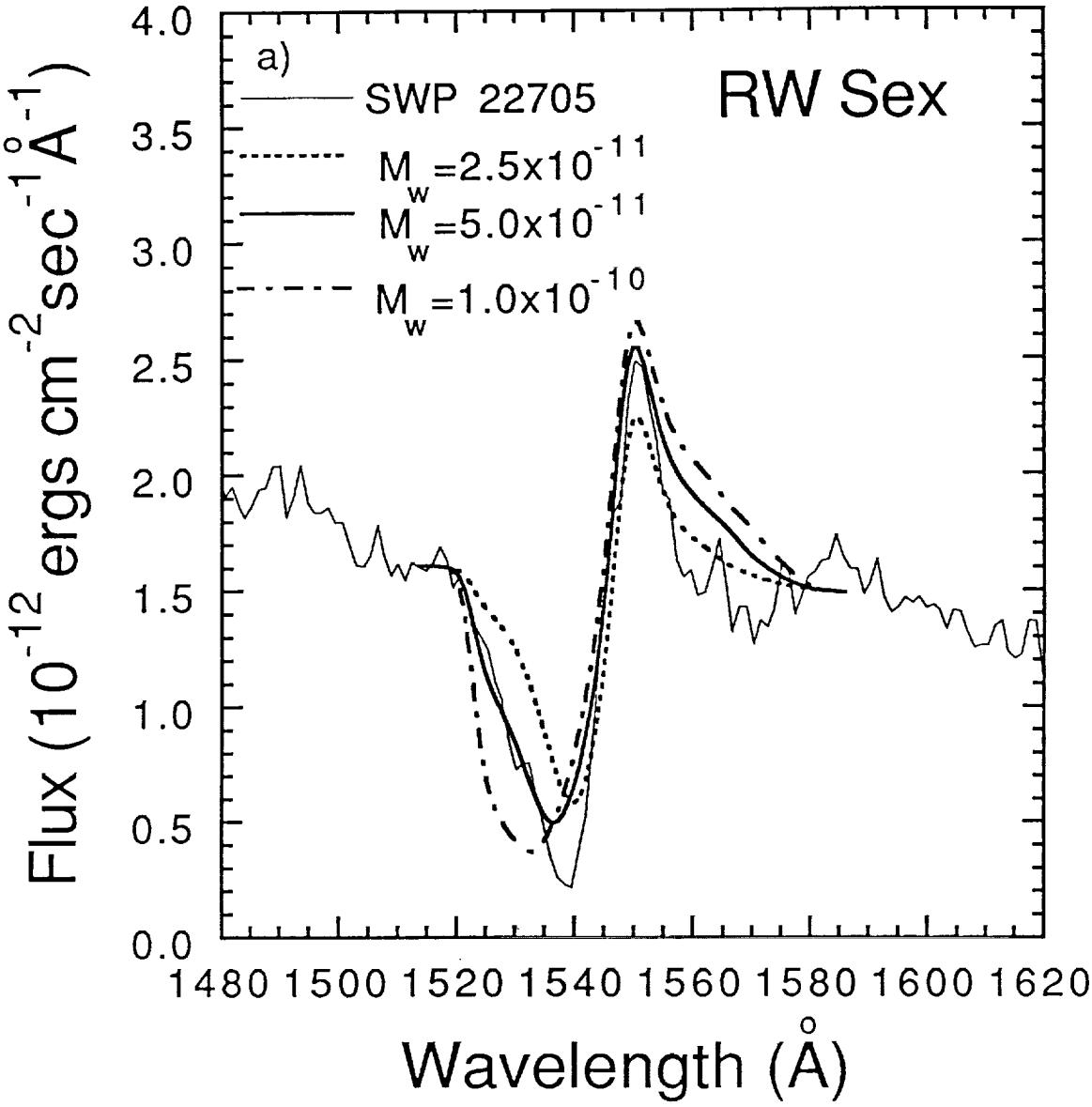
a)
SWP 22705
RW Sex
M_w=2.5x10^{-11}
M_w=5.0x10^{-11}
M_w=1.0x10^{-10}
Flux (10^{-12} ergs cm^{-2}sec^{-1}Å^{-1})
Wavelength (Å)
4.0
3.5
3.0
2.5
2.0
1.5
1.0
0.5
0.0
1480 1500 1520 1540 1560 1580 1600 1620

Figure. 7a

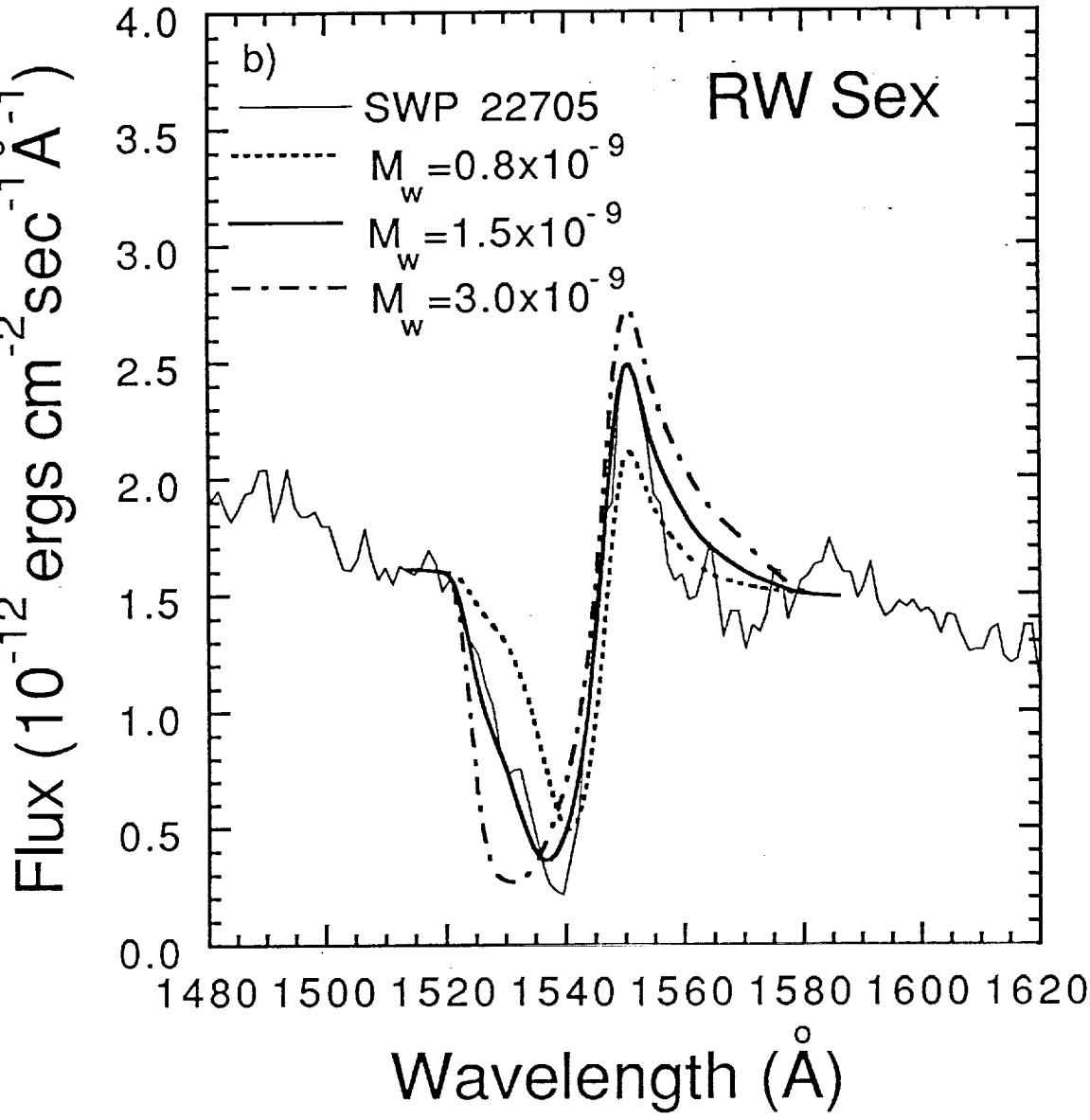
b)
SWP 22705
RW Sex
M_w=0.8x10^{-9}
M_w=1.5x10^{-9}
M_w=3.0x10^{-9}
Flux (10^{-12} ergs cm^{-2}sec^{-1}Å^{-1})
Wavelength (Å)
4.0
3.5
3.0
2.5
2.0
1.5
1.0
0.5
0.0
1480 1500 1520 1540 1560 1580 1600 1620

Figure. 7b

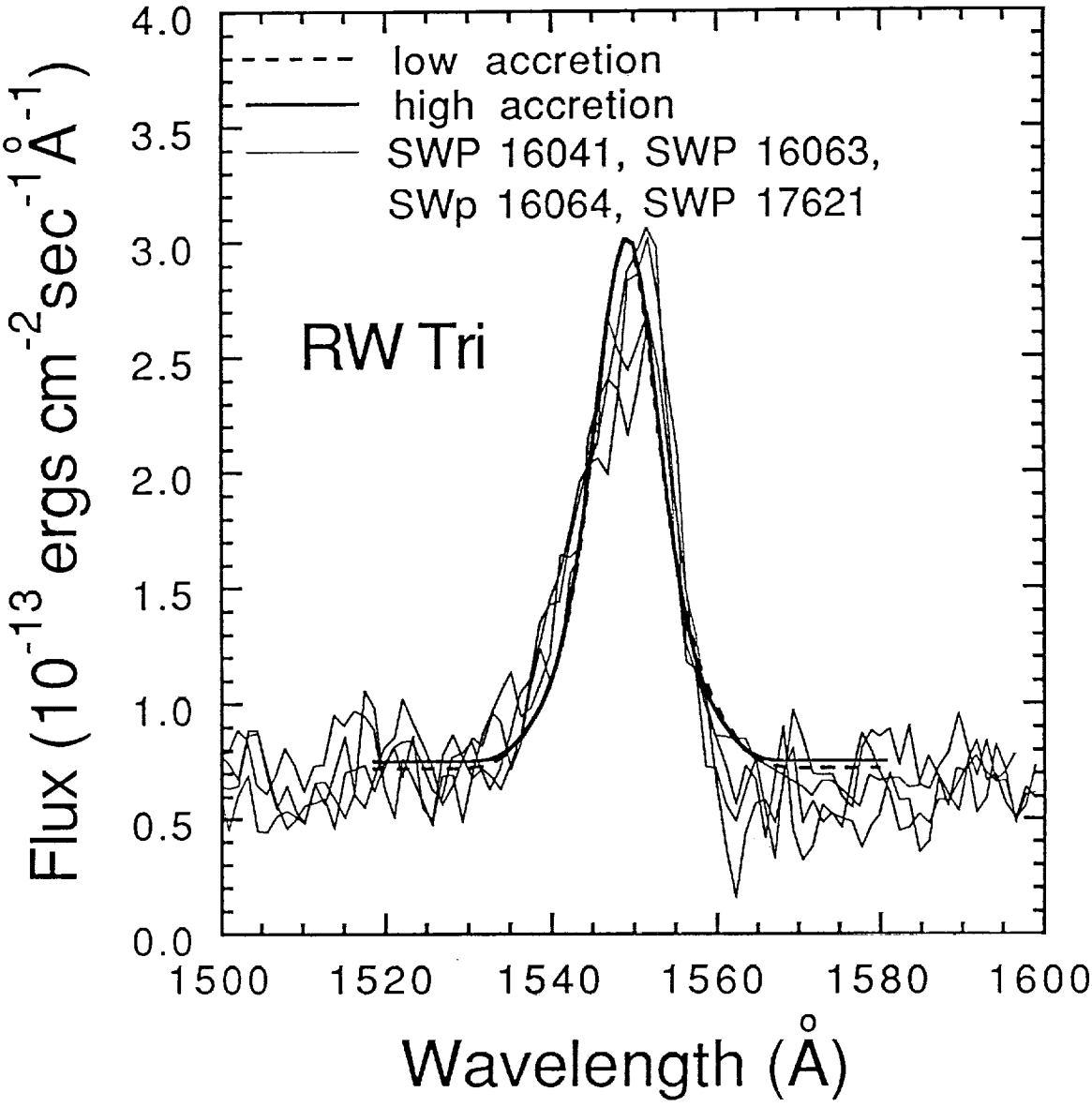
low accretion
high accretion
SWP 16041, SWP 16063,
SWp 16064, SWP 17621
RW Tri
Flux (10^{-13} ergs $cm^{-2}sec^{-1}Å^{-1}$)
Wavelength (Å)
4.0
3.5
3.0
2.5
2.0
1.5
1.0
0.5
0.0
1500
1520
1540
1560
1580
1600

Figure. 8

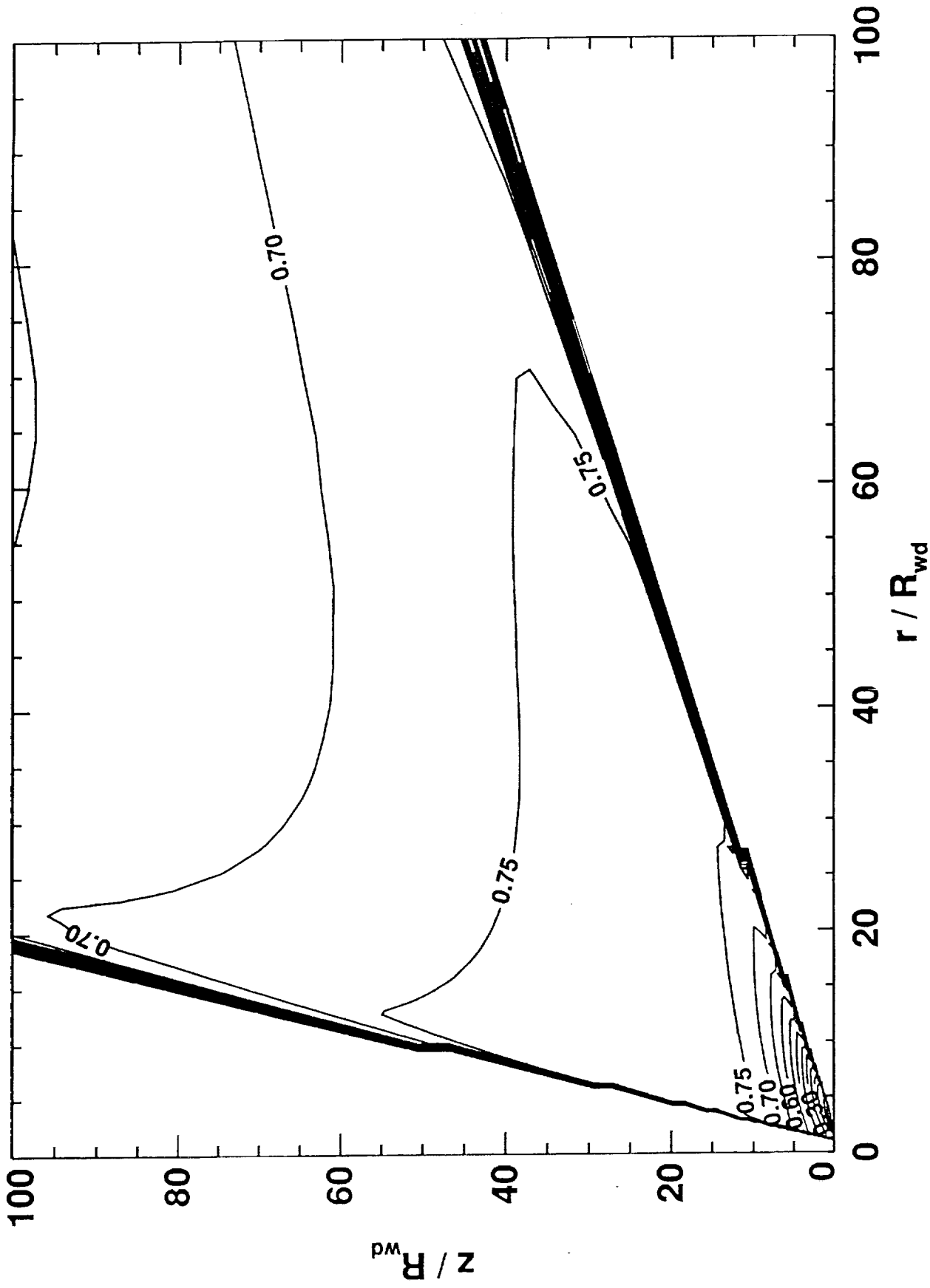
0.70
0.75
0.70
0.75
0.75
0.70
0.60
0
20
40
60
80
100
r / R_wd
0
20
40
60
80
100
z / R_wd

Figure 9a

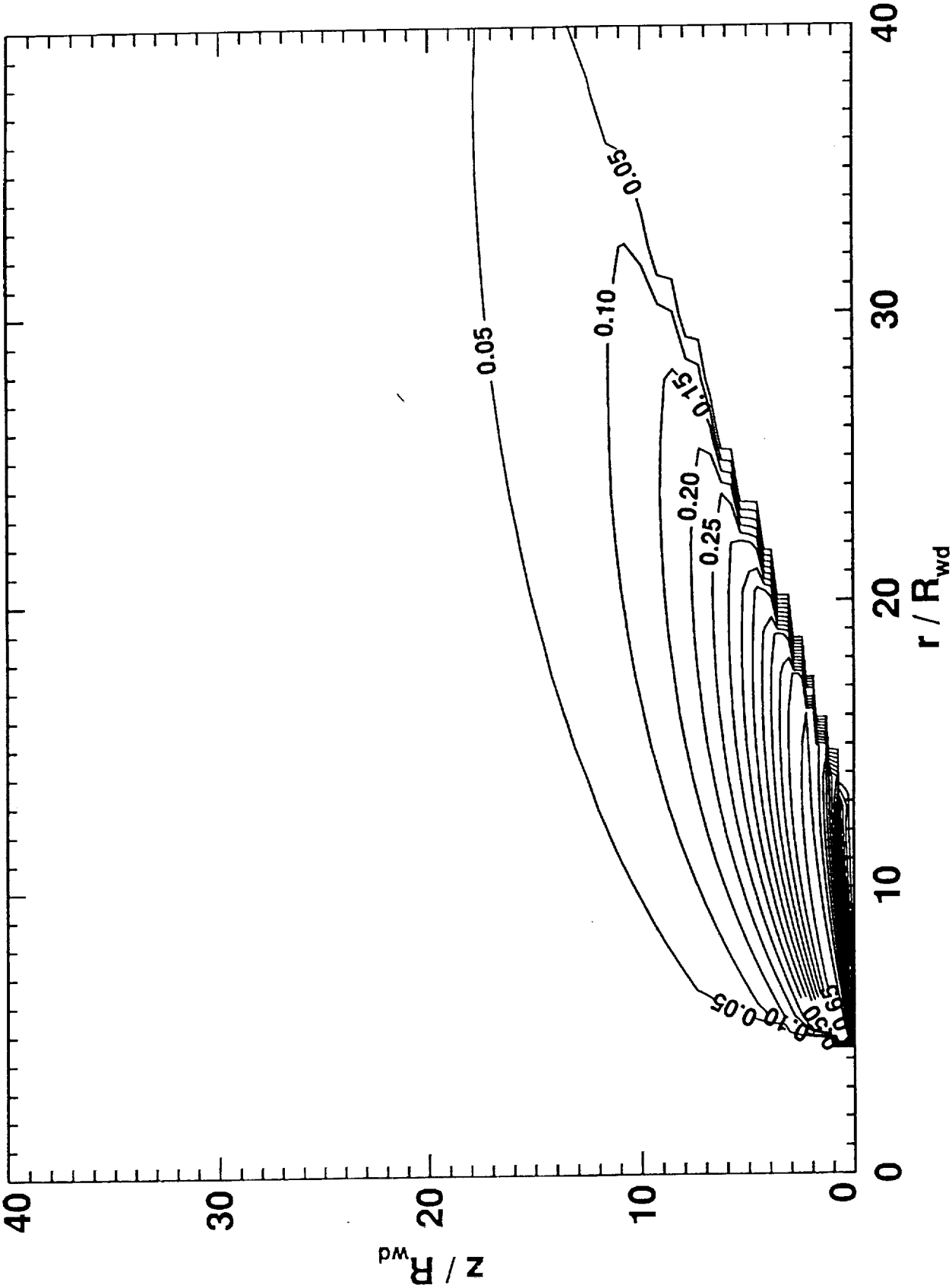

Figure 9b

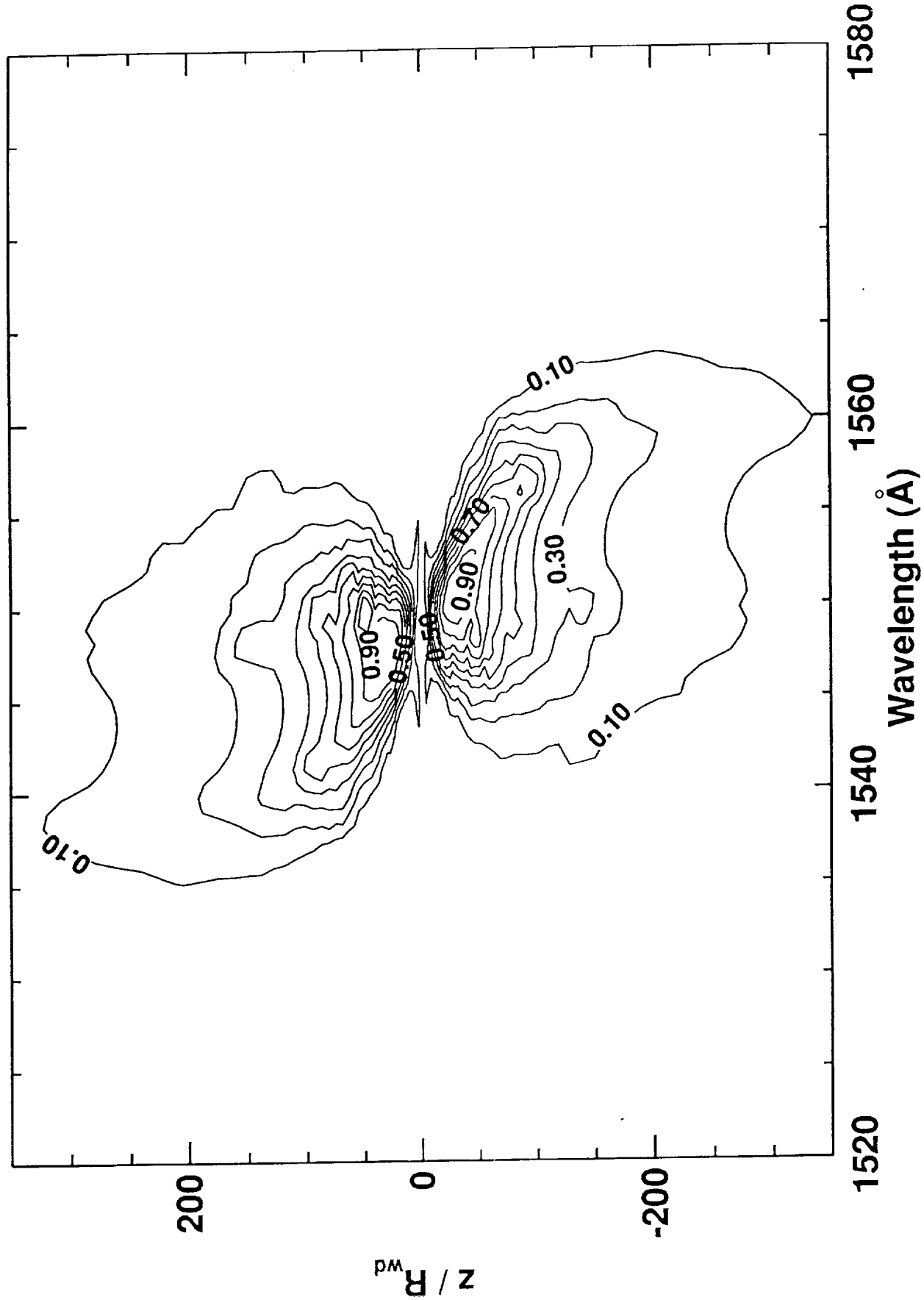
1580
1560
1540
1520
Wavelength (Å)
200
0
-200
z / R_wd
0.10
0.30
0.50
0.70
0.90

Figure 10a

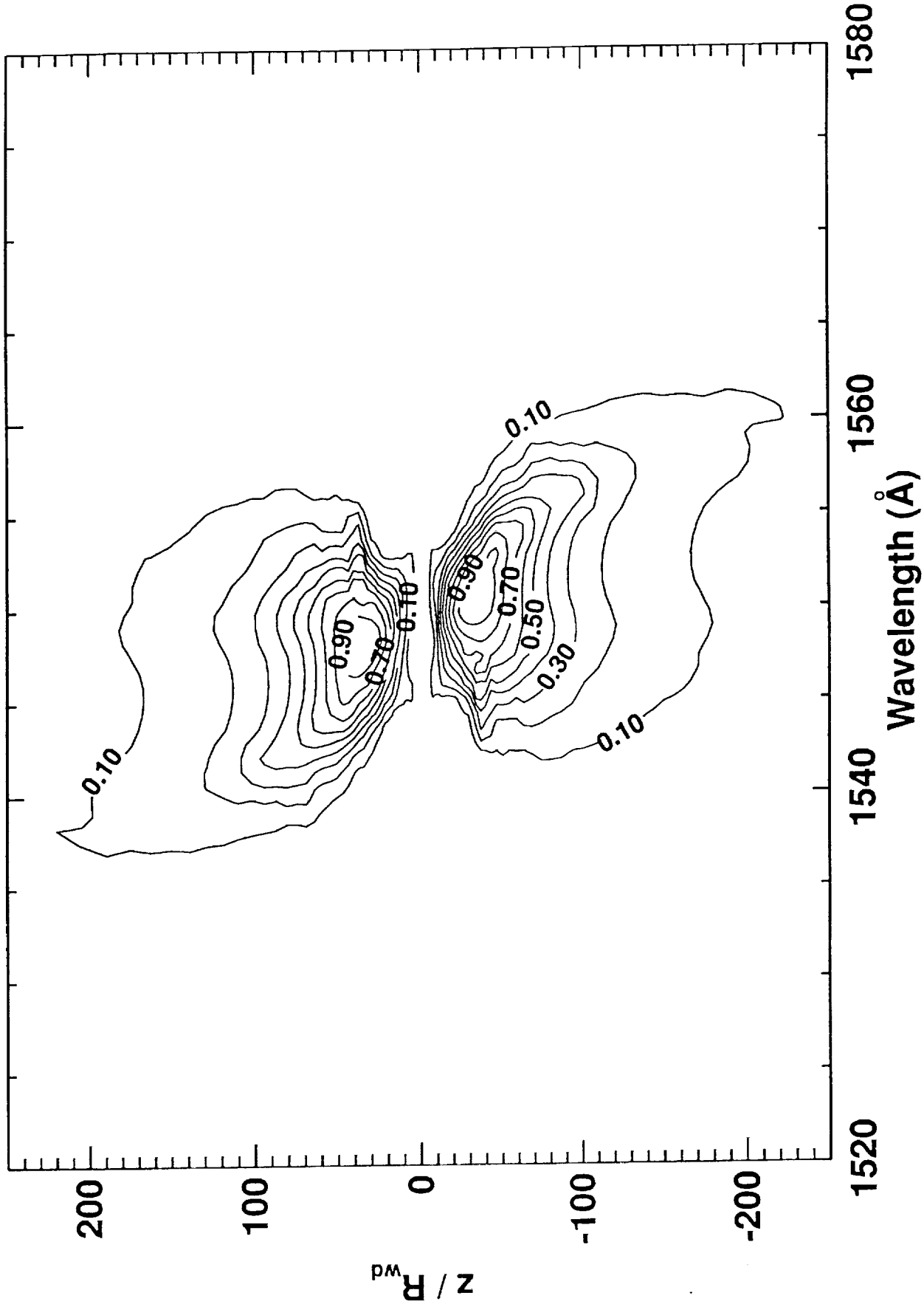
1580
1560
1540
1520
Wavelength (Å)
200
100
0
-100
-200
Z / R_wd
0.10
0.90
0.70
0.50
0.30
0.10
0.90
0.70
0.10
0.10

Figure 10b

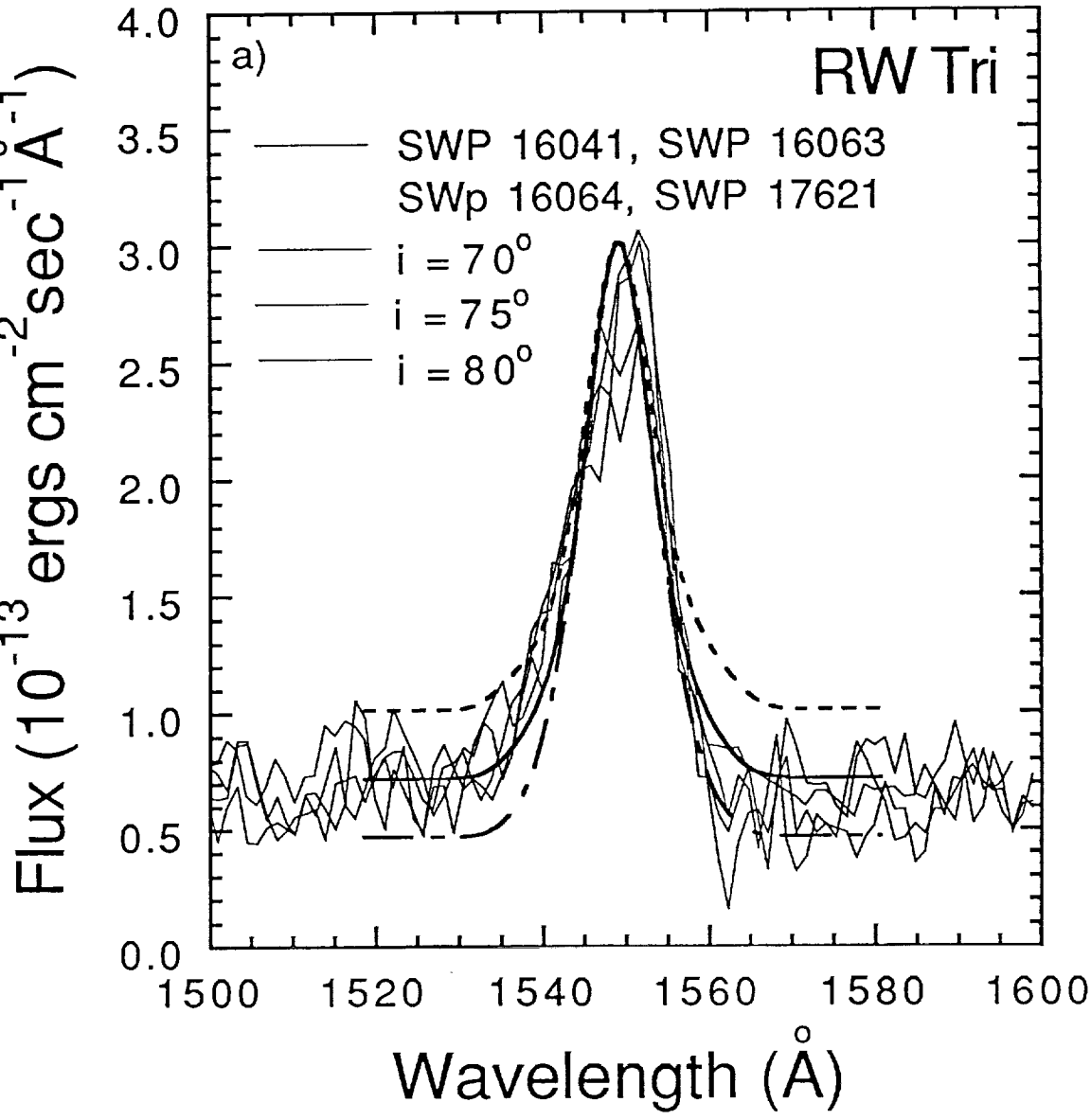
a)
RW Tri
SWP 16041, SWP 16063
SWp 16064, SWP 17621
i = 70°
i = 75°
i = 80°
Flux (10^{-13} ergs cm^{-2}sec^{-1}Å^{-1})
Wavelength (Å)
4.0
3.5
3.0
2.5
2.0
1.5
1.0
0.5
0.0
1500
1520
1540
1560
1580
1600

Figure. 11a

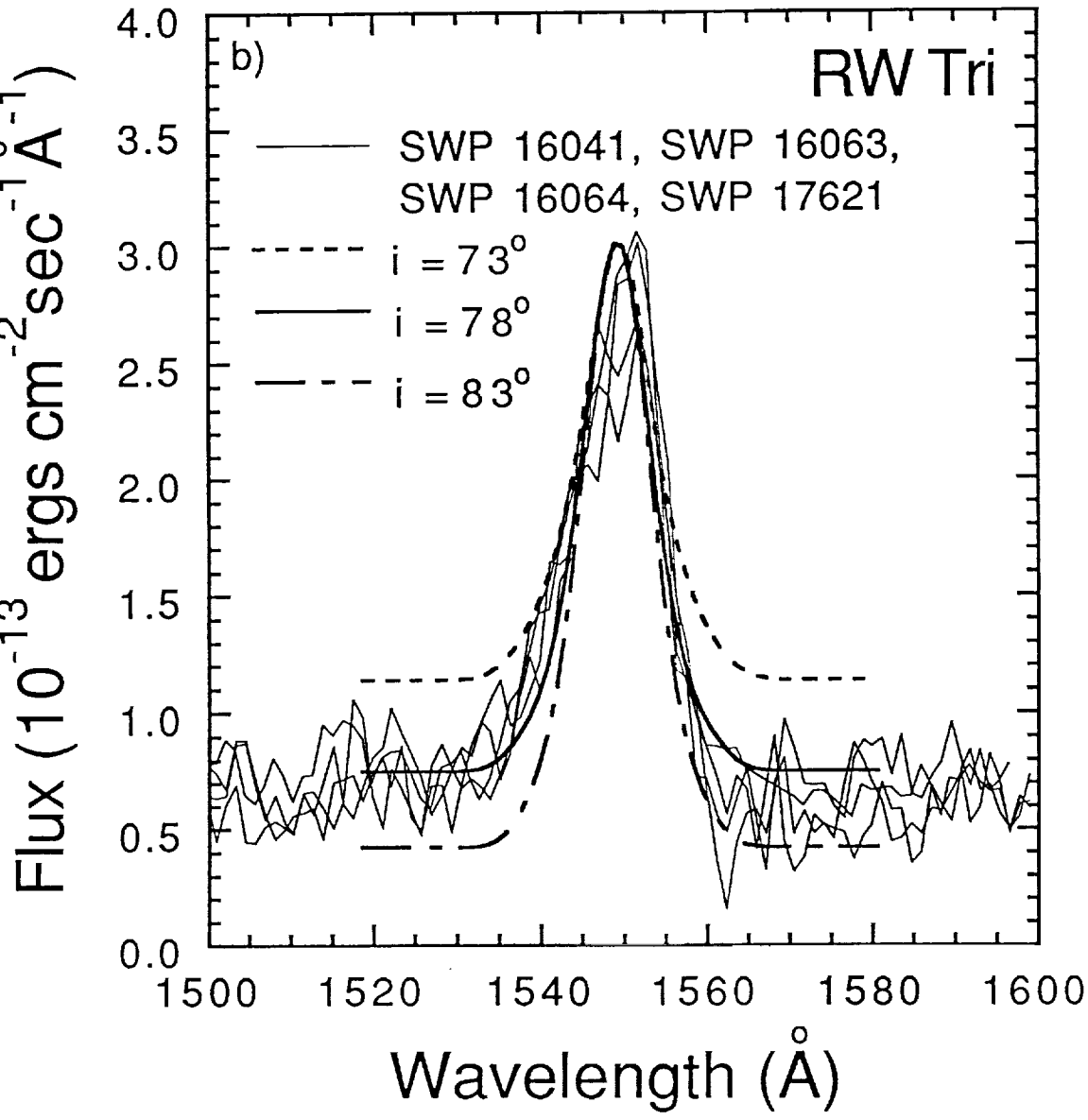
b)
RW Tri
SWP 16041, SWP 16063,
SWP 16064, SWP 17621
i = 73°
i = 78°
i = 83°
Flux (10^{-13} ergs cm^{-2}sec^{-1}Å^{-1})
Wavelength (Å)
4.0
3.5
3.0
2.5
2.0
1.5
1.0
0.5
0.0
1500
1520
1540
1560
1580
1600

Figure. 11b

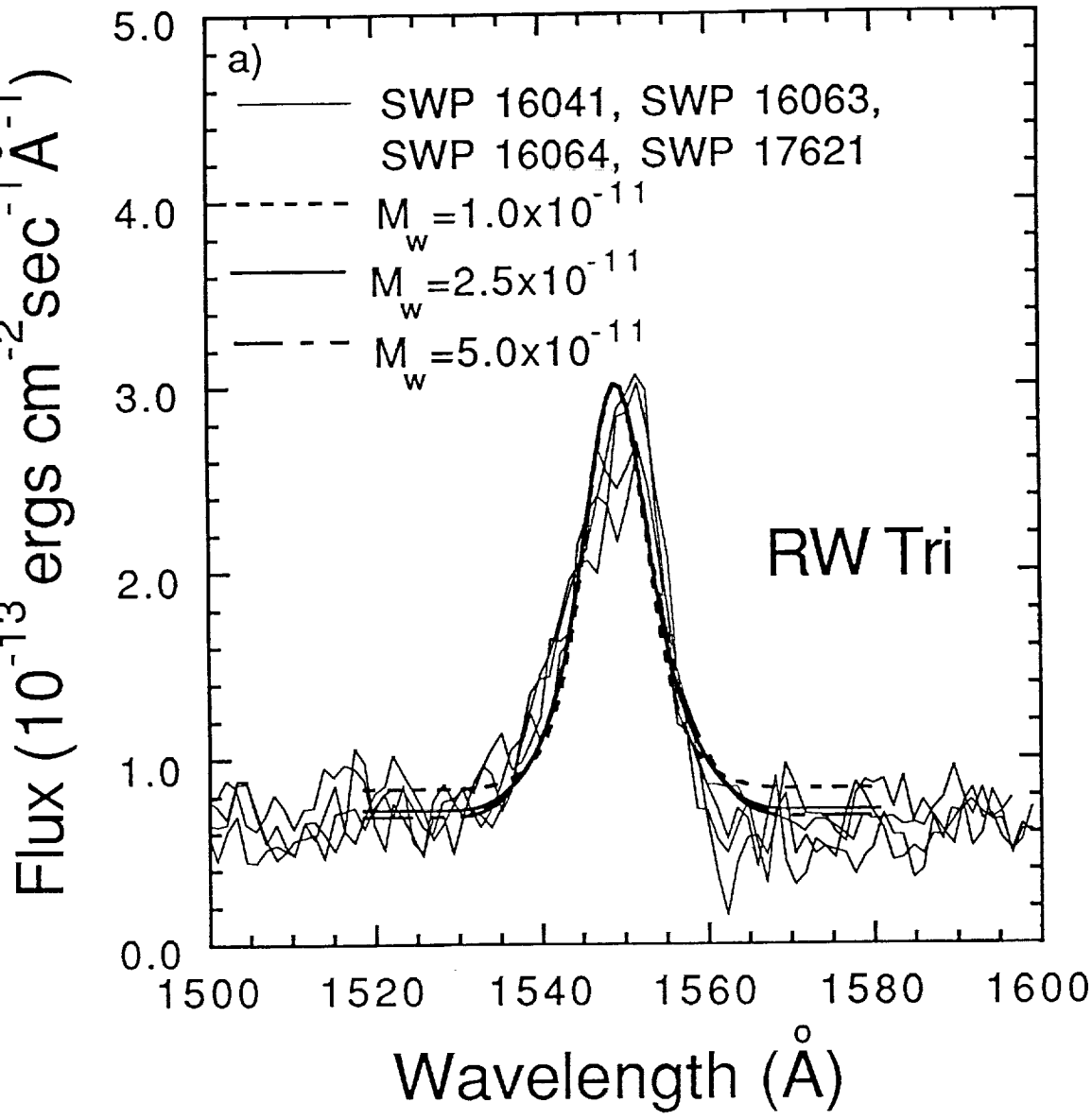
a)
SWP 16041, SWP 16063,
SWP 16064, SWP 17621
M_w=1.0x10^-11
M_w=2.5x10^-11
M_w=5.0x10^-11
RW Tri
Flux (10^-13 ergs cm^-2 sec^-1 Å^-1)
Wavelength (Å)
5.0
4.0
3.0
2.0
1.0
0.0
1500
1520
1540
1560
1580
1600

Figure. 12a

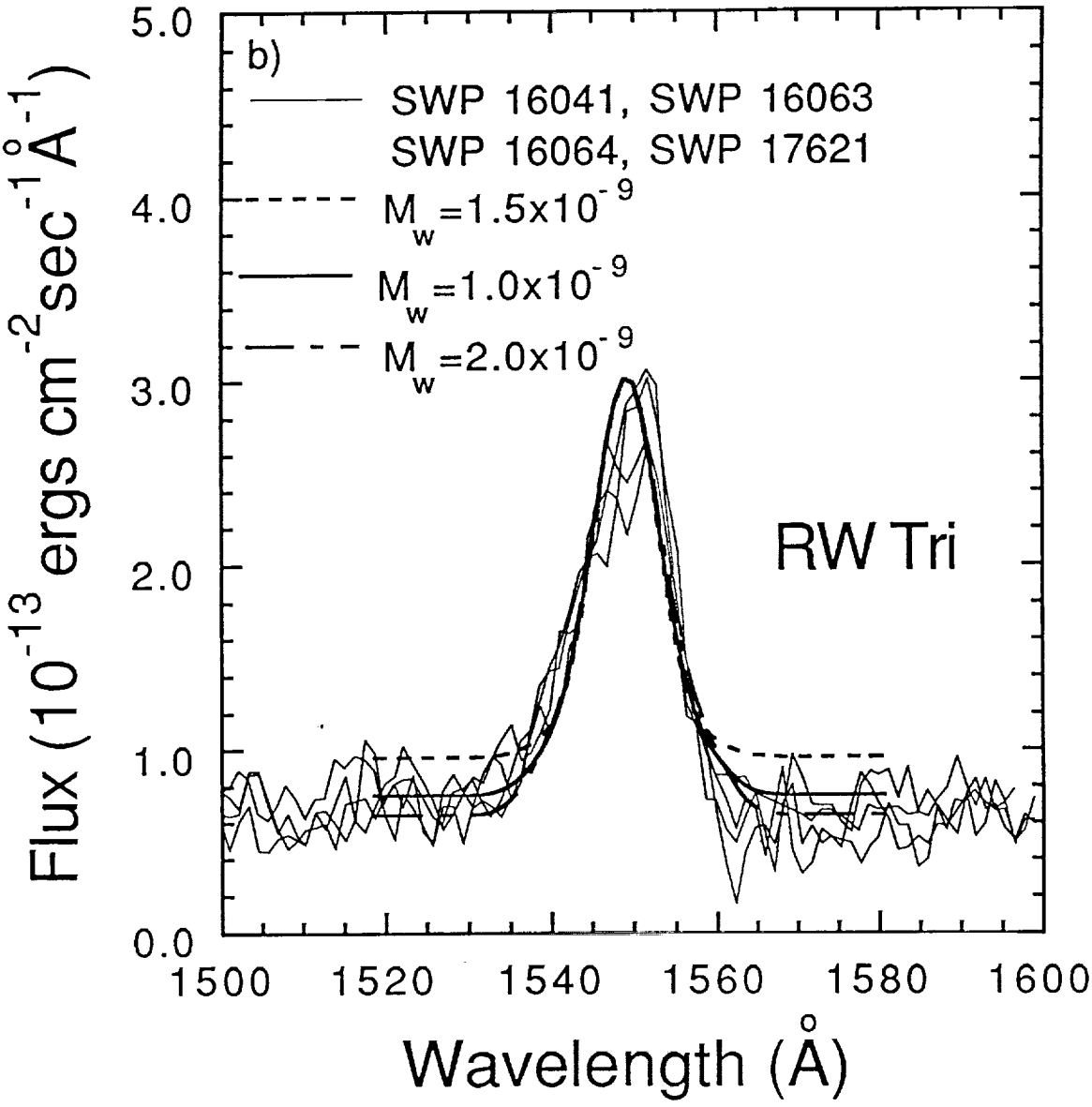
b)
SWP 16041, SWP 16063
SWP 16064, SWP 17621
M_w=1.5x10^-9
M_w=1.0x10^-9
M_w=2.0x10^-9
RW Tri
Flux (10^-13 ergs cm^-2 sec^-1 Å^-1)
Wavelength (Å)
5.0
4.0
3.0
2.0
1.0
0.0
1500
1520
1540
1560
1580
1600

Figure. 12b

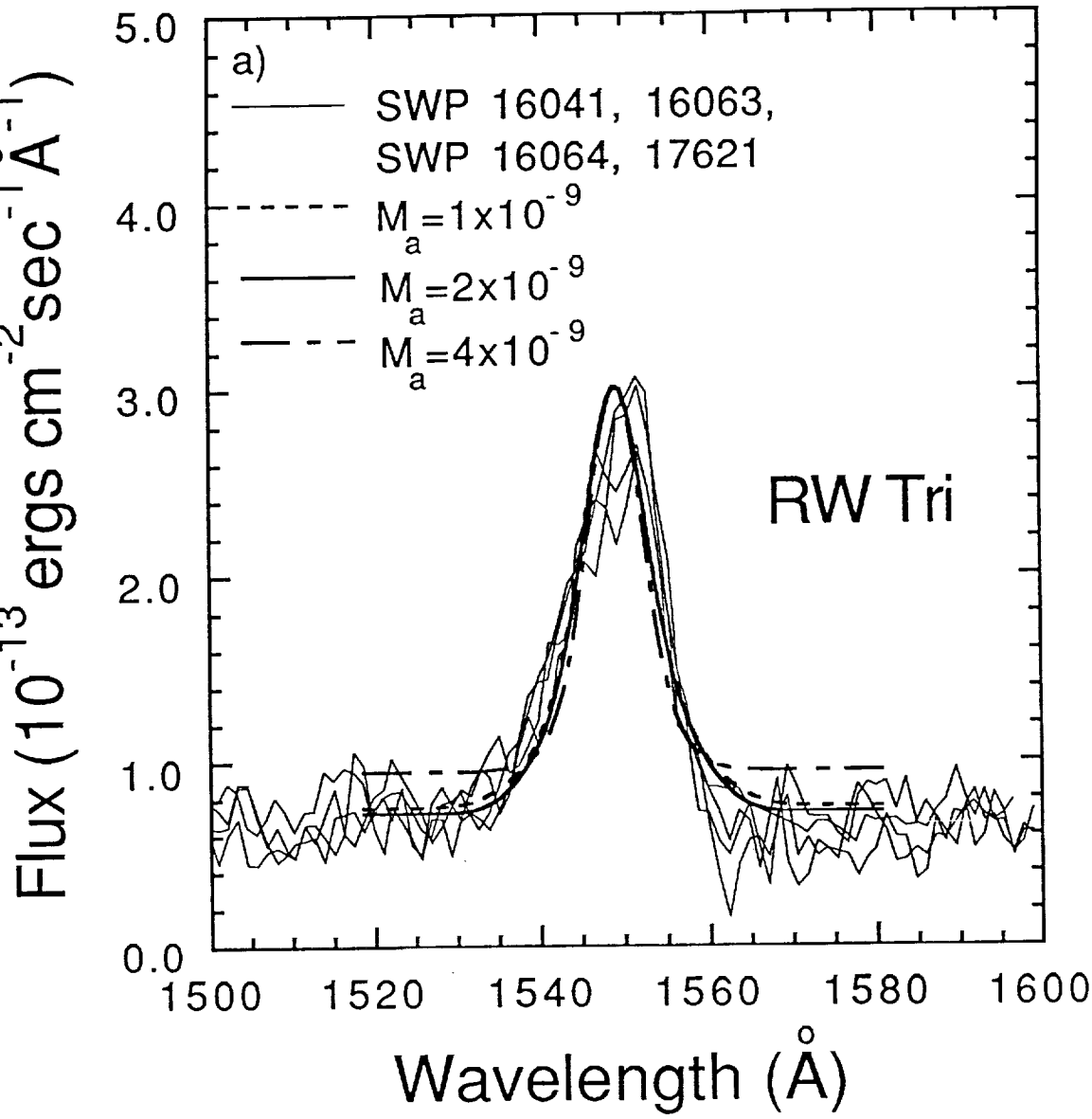
a)
SWP 16041, 16063,
SWP 16064, 17621
$M_a=1x10^{-9}$
$M_a=2x10^{-9}$
$M_a=4x10^{-9}$
RW Tri
Flux (10^{-13} ergs cm^{-2}sec^{-1}Å^{-1})
Wavelength (Å)
5.0
4.0
3.0
2.0
1.0
0.0
1500
1520
1540
1560
1580
1600

Figure. 13a

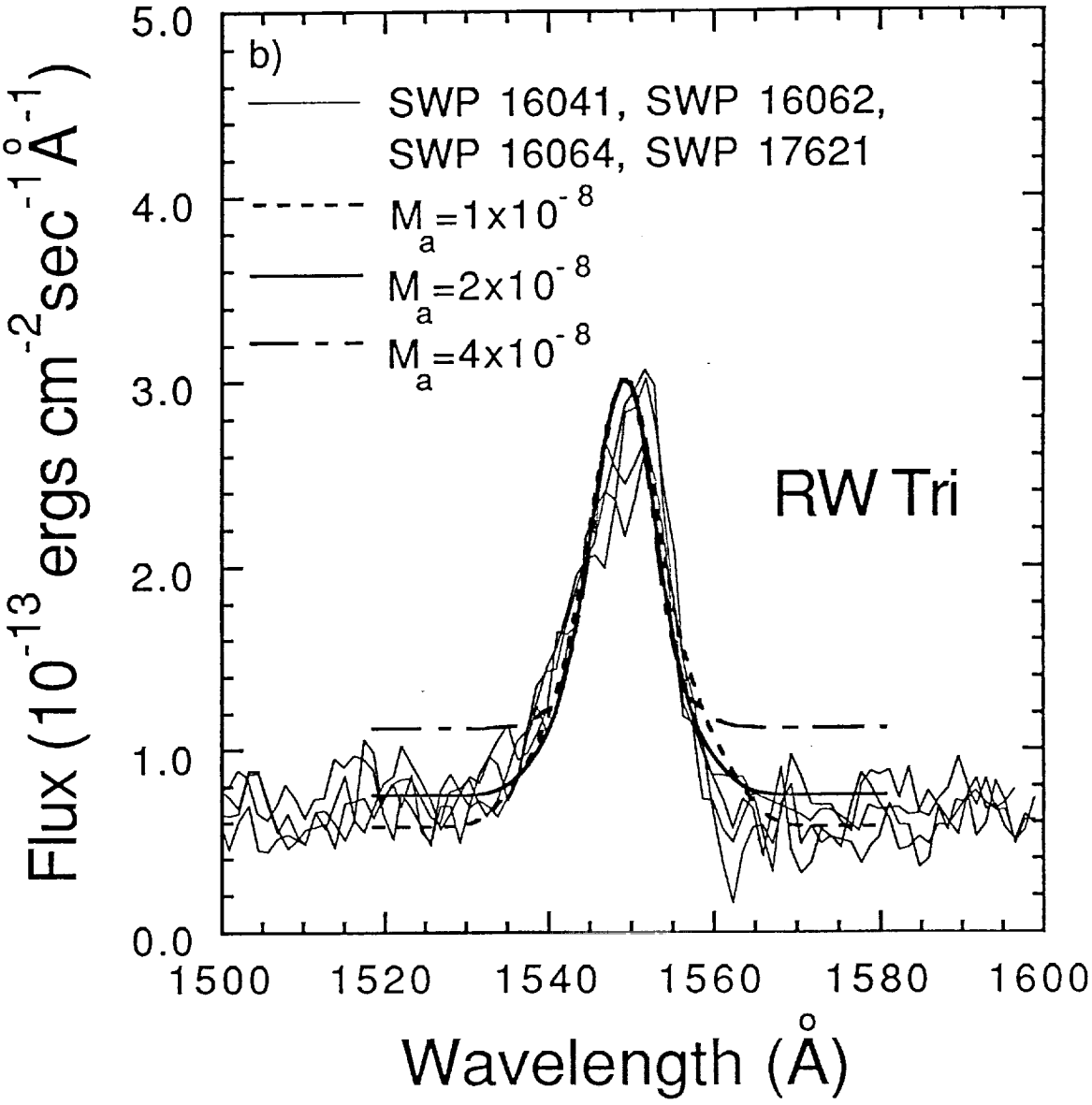
b)
SWP 16041, SWP 16062,
SWP 16064, SWP 17621
M_a=1x10^-8
M_a=2x10^-8
M_a=4x10^-8
RW Tri
Flux (10^-13 ergs cm^-2 sec^-1 Å^-1)
Wavelength (Å)
5.0
4.0
3.0
2.0
1.0
0.0
1500
1520
1540
1560
1580
1600

Figure. 13b

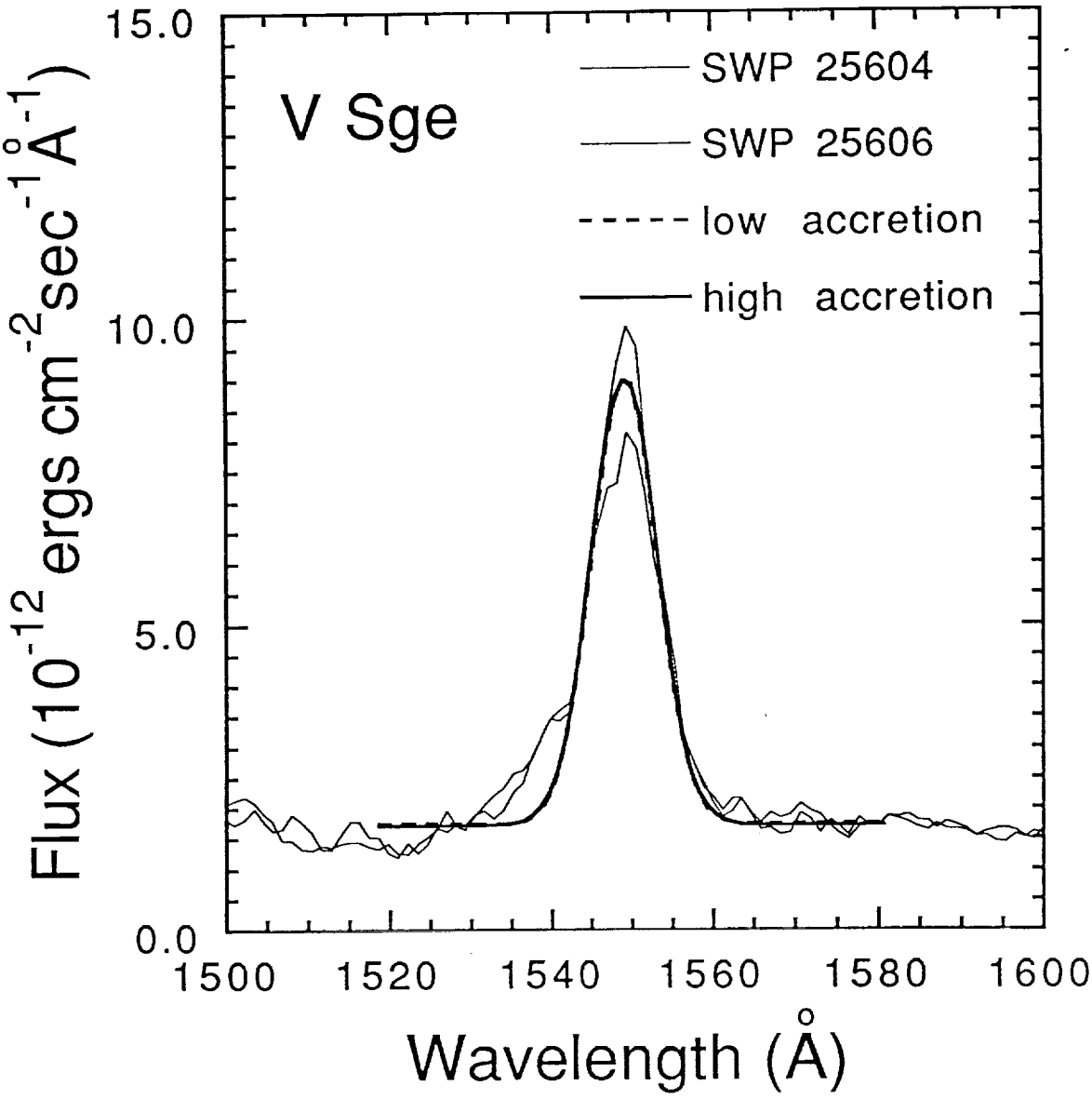
V Sge
SWP 25604
SWP 25606
low accretion
high accretion
Flux (10^{-12} ergs cm^{-2}sec^{-1}Å^{-1})
15.0
10.0
5.0
0.0
1500
1520
1540
1560
1580
1600
Wavelength (Å)

Figure. 14

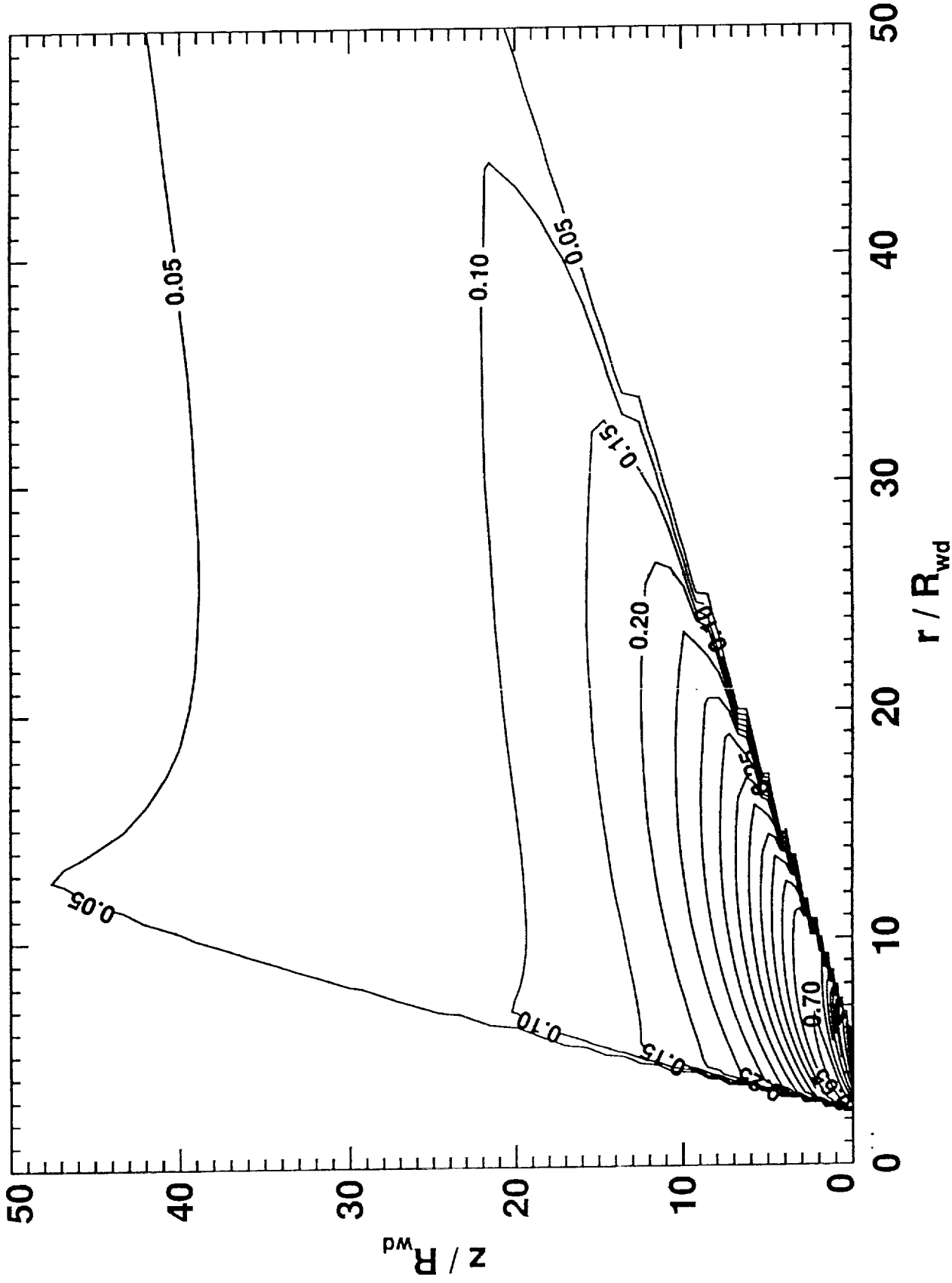
0.05
0.10
0.05
0.15
0.20
0.10
0.05
0.70
0.65
0.60
0.55
0.50
0.45
0.40
0.35
0.30
0.25
0.20
0.15
0.10
0.05
0
10
20
30
40
50
r / R_wd
z / R_wd

Figure 15a

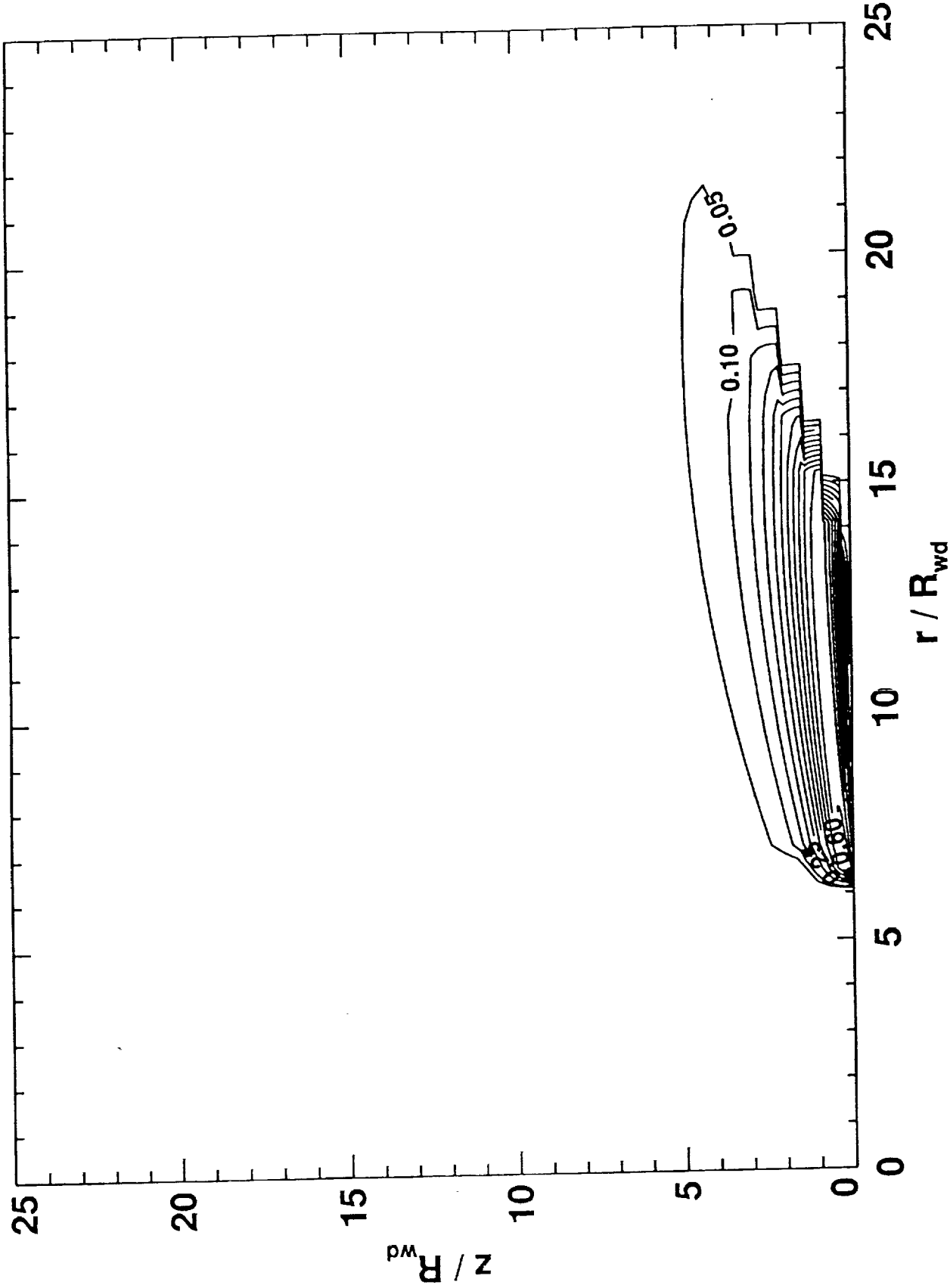

Figure 15b

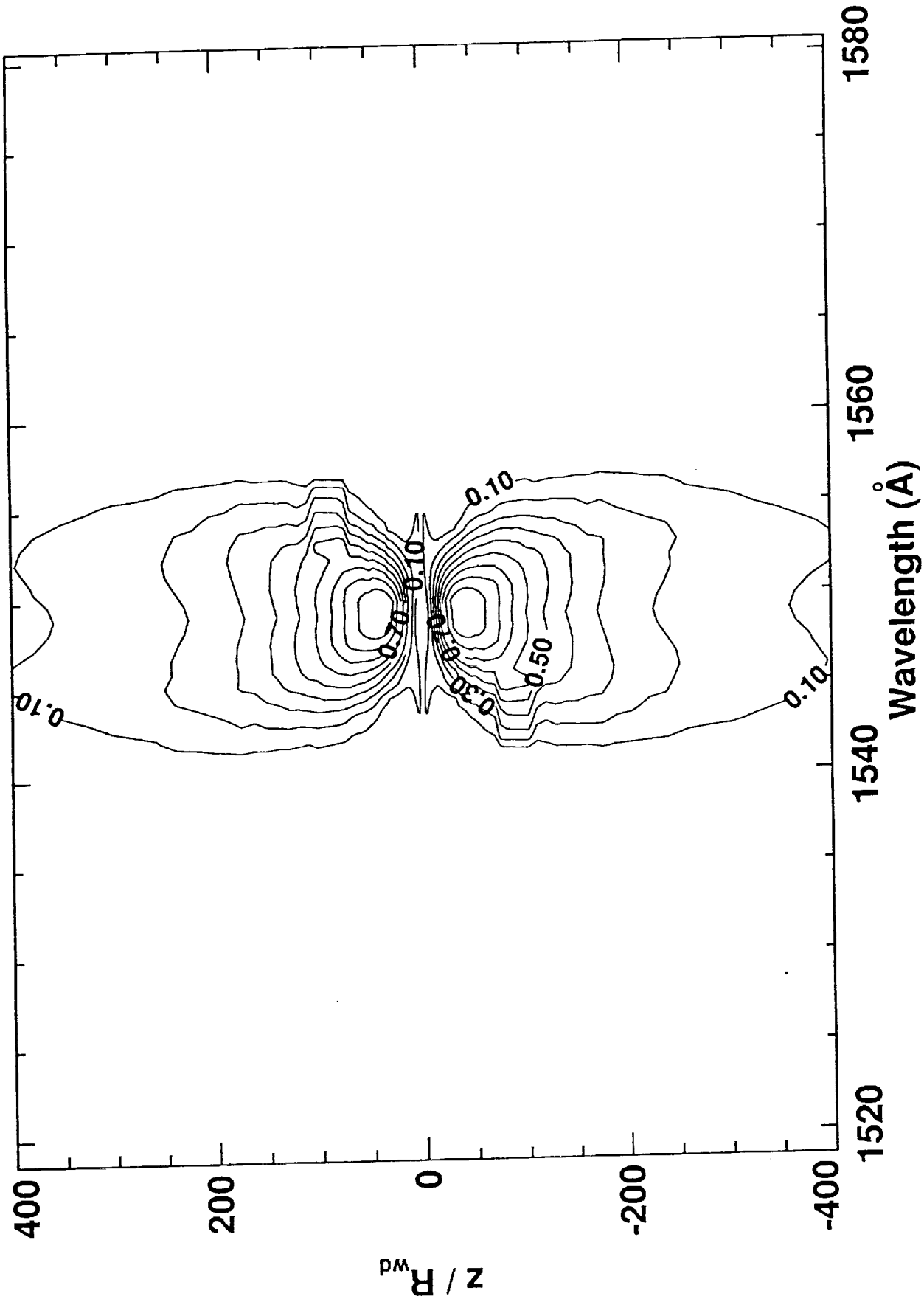
1580
1560
1540
1520
Wavelength (Å)
400
200
0
-200
-400
z / R_wd
0.10
0.10
0.20
0.20
0.30
0.50
0.10
0.10

Figure 16a

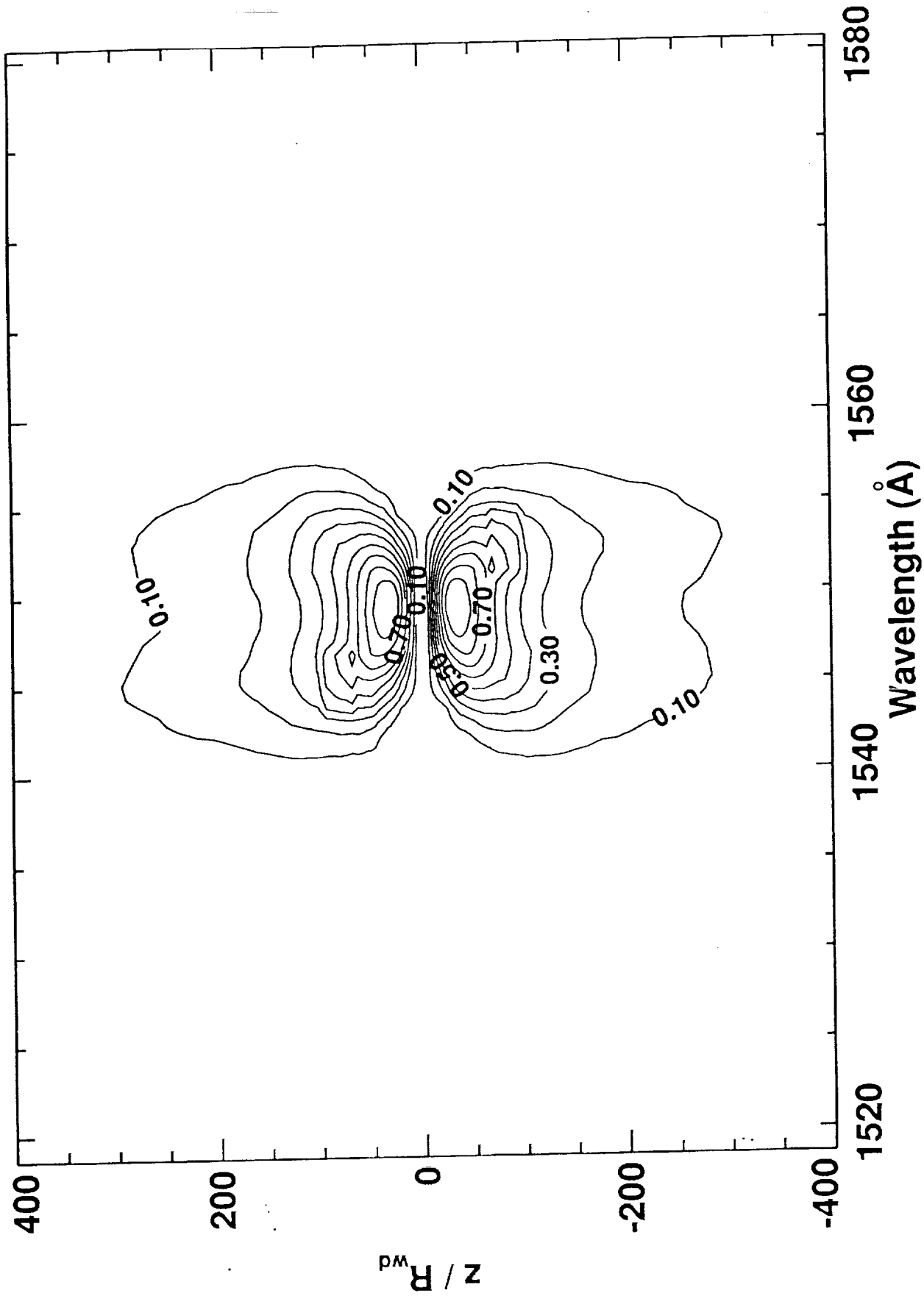
0.10
0.70
0.30
0.50
400
200
0
-200
-400
z / R_wd
1520
1540
1560
1580
Wavelength (Å)

Figure 16b